Chapter 1 Introduction

1.1 Introduction to nanotechnologies for one-dimensional nanostructures

Nanostructures, structures that have at least one dimension between 1 and 100 nm, have received much interest due to their peculiar and fascinating properties and applications superior to their bulks. [1.2.3]   There are two major aspects: "top-down" and "bottom-up" techniques as shown in Fig.1-1 to fabricate one-dimensional structures of nanometer-length scale.
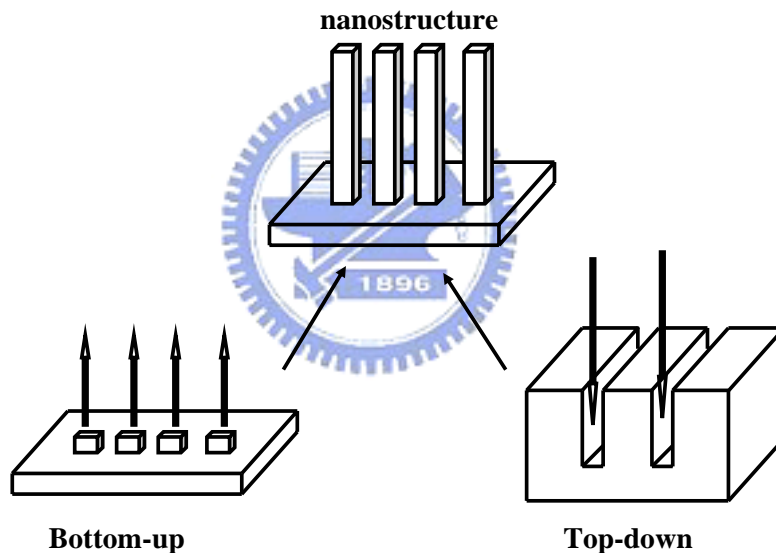

Fig. 1-1 Diagram of top-down and bottom-up.

One-dimension semiconductor nanostructures such as nanowires, nanotubes, nanobelts, nanocombs, nanocantilevers, and nanosprings [4-9] have been fabricated by the bottom-up methods such as chemical vapor deposition (CVD), laser ablation, vapor phase evaporation, and solution and template based methods. [10-14] Different kinds of one dimensional semiconductor nanostructures have been developed and applied to various nanoscale devices, such as nanotransistor, nano-logic gate, nanophotonics, nano-laser source, nano-grating, and nanoscale
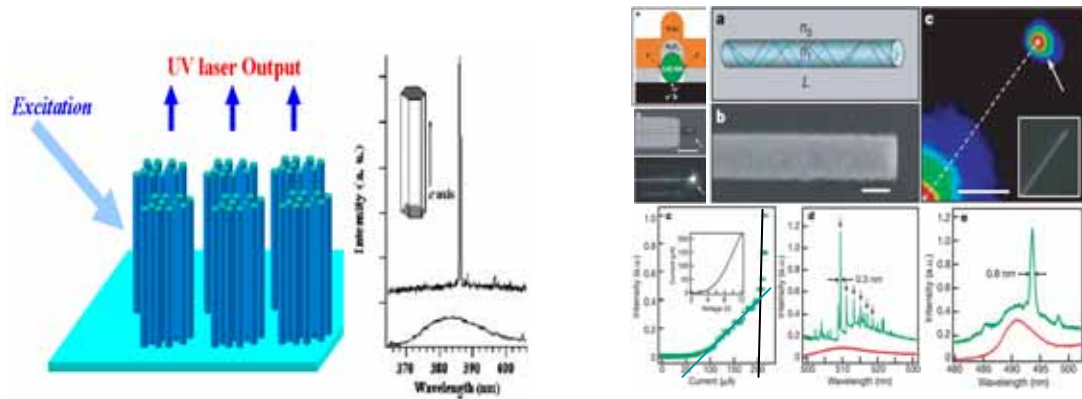
photonics integration Fig. 1-2 (a)~(e)

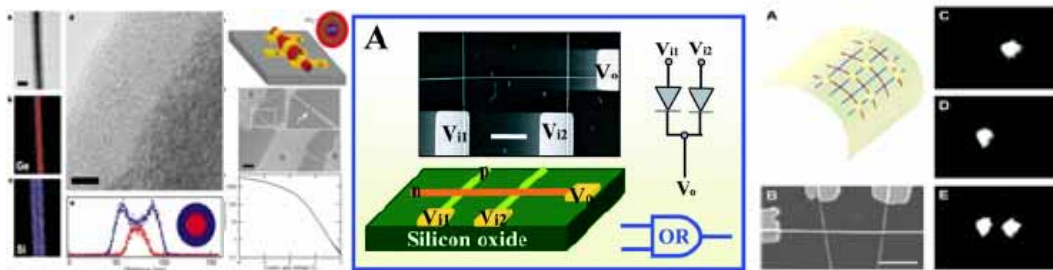Fig. 1-2 Nanowires (a) optically driven nanolaser [15] (b) electrically driven nanolaser [16]

Fig. 1-2 (c) Coaxially-gated nanowire transistors [17] (d) Nano-logicgate [18] (e) Nanophotonics [19]

1.2 Properties of ZnO and ZnO-based compounds

The wurtzite structure of the ZnO crystal is shown in Fig 1-3 which has hexagonal structure with the lattice constant of $a=3.249$ Å, $c=5.207$ Å. The basic properties of ZnO for optoelectronic applications can be obtained by examining Table I, which compares the relevant material properties of ZnO with those of other wide band gap semiconductors. The notable properties are the large bond strength (indicated by the cohesive energy) and the melting point and the extreme stability of excitons (indicated by the large exciton binding energy). ZnO is one of the "hardest" materials in the Ⅱ-Ⅵ compound family.
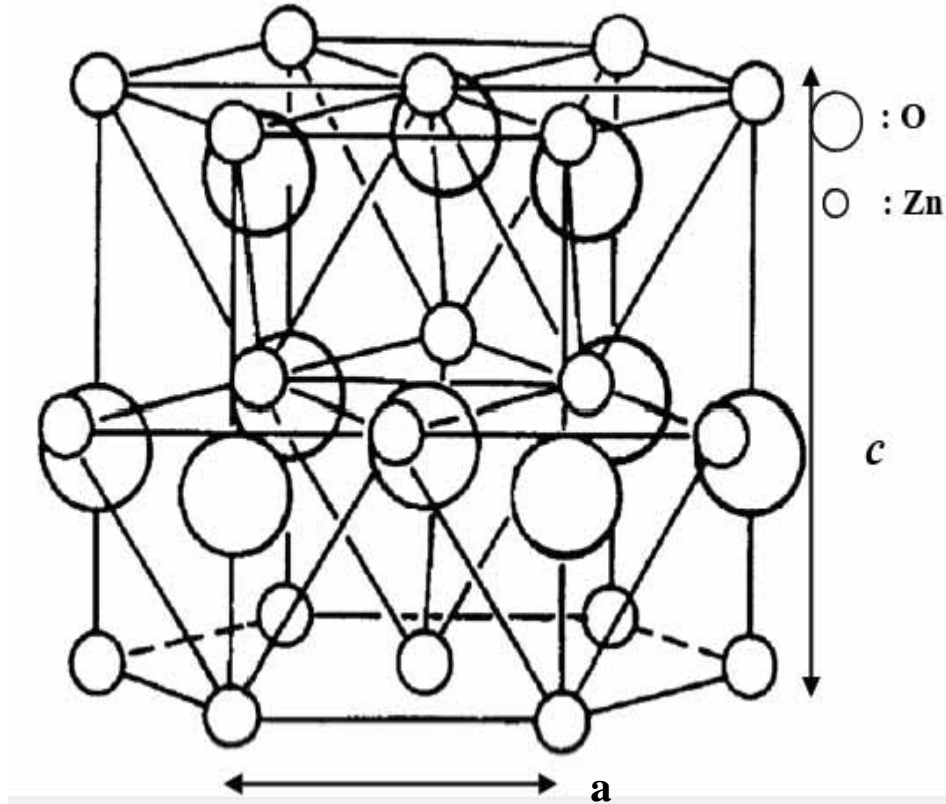
Fig 1-3 ZnO wurtzite structure

Table Ⅰ. Comparison of properties of ZnO with those of other wide band gap semiconductors. [20]

Material	Crystal structure	Lattice constants		Band gap energy at RT	Cohesive energy	Melting point	Exciton binding energy	Dielectric constants	
		a (Å)	c (Å)	E_g (eV)	E_{coh} (eV)	T_m (K)	E_b (meV)	$\varepsilon(0)$	$\varepsilon(\infty)$
ZnO	Wurtzie	3.249	5.207	3.37	1.89	2248	60	8.75	3.75
ZnS	Wurtzie	3.823	6.261	3.8	1.59	2103	39	9.6	5.7
ZnSe	Zinc blende	5.668	⋯	2.70	1.29	1793	20	9.1	6.3
GaN	Wurtzie	3.189	5.185	3.39	2.24	1973	21	8.9	5.35
6H-SiC	Wurtzie	3.081	15.117	2.86(ind.)	3.17	>2100	⋯	9.66	6.52

ZnO has attracted considerable scientific and technological attention due to its wide direct bandgap semiconductor of 3.37 eV that is suitable for blue and ultraviolet (UV) optoelectronic applications.   In this regard, a large exciton binding energy of ZnO is 60 meV, which is significantly larger than that of ZnSe (22 meV) and GaN (25 meV).   Therefore, exciton stability of ZnO provides opportunities for making highly

efficient optoelectronic devices at room temperature (thermal energy 26meV), and therefore enables stable existence of excitons at room temperature even up to 550^0C. The stable excitons could lead to laser action based on their recombination even at temperature well above room temperature.

Recently, UV lasing for ZnO nanowires has also been demonstrated at room temperature [21]. It is expected that a lower threshold optical pumping density for lasing is due to the carrier confinement effect in one dimensional nanowires. ZnO nanowires have been evaluated for potential application as UV laser [22], light-emitting diodes [23], and UV photodetectors [24, 25], and array gratings. In recent years, much effort has been devoted to developing various 1-D ZnO nanostructures. Vapour-liquid-solid (VLS) and vapour-solid (VS) mechanisms for growth of ZnO nanowires are well recognized and have been used.

1.3 Motivation

1.3.1 Problems of previous growth techniques

There are some problems to use the methods of vapour-liquid-solid (VLS) and vapour-solid (VS) for growth ZnO nanostructures. Usually, there are more than one morphologies can be observed. Many types of morphologies, such as thin film, nanowires, nanosheet and nanosaws, would confuse the investigation of one dimension ZnO nanostructures.

1.3.2 Growth mechanisms and control morphology

Synthesis of ZnO nanowires by simple vapor transition deposition always appear two structures--buffer layer and nanowires. In the process of growth ZnO nanowires by vapor transition deposition, one heats the reaction source and the substrate together. At the low temperature if prefers to grow 2-D ZnO structures and the high

temperature if prefers to grow 1-D ZnO structures[26] as shown is Fig 1-4. By simple vapor transition deposition the synthetic Zn gas is produced before the temperature has arrived at the target temperature. Recently, before offering the compound gas that is preheated the substrate to the aim temperature, that can successfully controll different type of single morphology of CdSe nanostructure [27].
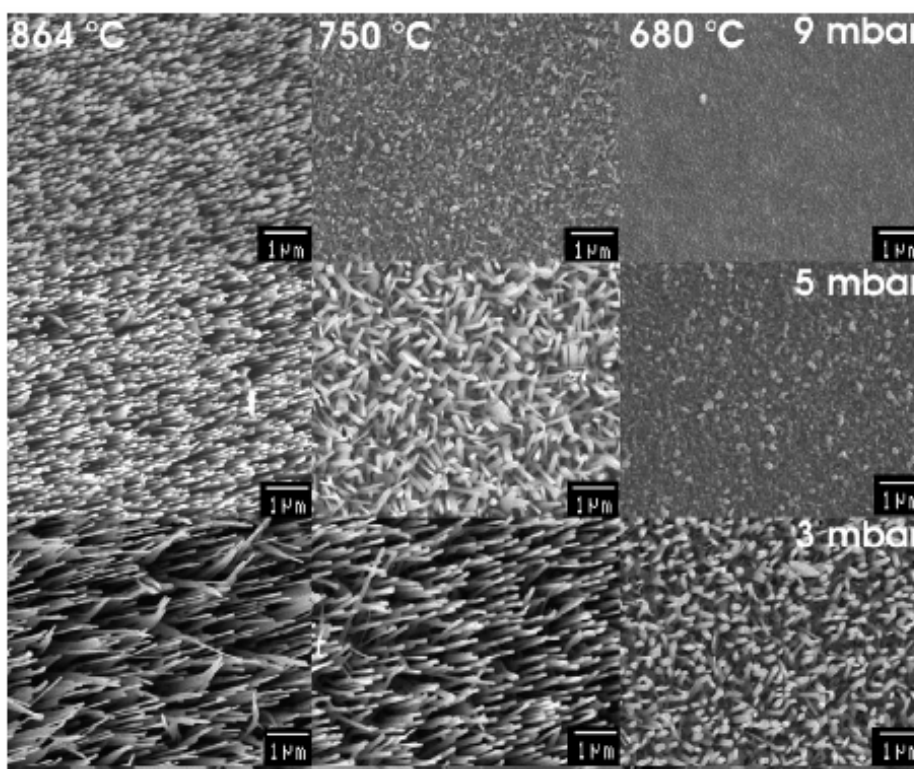

Fig 1-4. ZnO structures grown at different conditions using the same gas flow and Au catalyst .[27]

By using the same technique, to preheat the substrate to growth ZnO nanostructure is a simple method to improved the vapor transition deposition that may obtain a single morphology of ZnO nanostructures. The improvement in vapor transition deposition provides a way of eliminating the buffer layer during growing ZnO nanowire by vapor transition deposition.

1.4 Organization of thesis

Beside this chapter, the thesis includes other four chapters. In Chapter 2 we

exhibit the theoretical background of the experiments such as the thermal vapor process, scanning electron microscopy (SEM), x-ray diffraction (XRD), Raman and photoluminescence (PL) spectroscopes, respectively.   In Chapter 3, we display the experimental details including the measurement apparatus and processes.   By means of the SEM, XRD, Raman, and PL spectroscopes, the morphology, the crystalline quality, and the optical emission properties of ZnO nanowires grown by non-preheating and preheating methods will be investigated and discussed in the Chapter 4.   Then we made a conclusion and future work in the final chapter.

References

[1] *Handbook of nanostructured materials and nano-technology(Ed: H.S. Nalwa)*, Acasmeic Press, New York 2000. *Nanostructured materials: clusters, composites, and thin film,* edited by V.M. Shalaev, M. Moskovits, American chemical society, Washington, DC 1997. *Nanomaterials: synthesis, properties, and applications*, edited by A.S. Edelstein, R.C. Cammarata, *Institute of physics, Philiadelphia*, PA 1996.

[2] A special issue on nanoscale materials, Acc. Chem. Res. 32 1999. P. Alivisatos, P.F. Barbara, A.W. Castleman, J. Chang, D.A. Dixon, M.L. Kline, G. L. McLendon, J.S. Miller, M.A. Ratner, P. J. Rossky, S.I. Stupp, M.I. Thompson, *Adv. Mater.*, **10**, 1297 (1998). Special issue on nanostructured materials, *Chem. Mater.*, **8**, 1569 (1996). G. A. Ozin, *Adv. Mater.*, **4**, 612 (1992).

[3] R. Dagani, C&EN News October, 27, 2000. A. Thiaville, J. Miltat, *Science*, **284**, 1939 (1999)

[4] Y.Y. Wu, H.Q. Yan, M.H. Huang, B. Messer, J.H. Song, and P.D. Yang, *Chem. Eur. J.*, **8**,1261 (2002).

[5] H. Murakami, M. Hirakawa, C. Tanaka, and H. Yamakawa, *Appl. Phys. Lett.*, **76**, 1776 (2000).

[6] Z.R. Dai, Z.W. Pan, and Z.L. Wang, *Adv. Func. Mater.*, **13**, 9 (2003).

[7] Y.H. Leung, A.B. Djurišic, J. Gao, M.H. Xie, Z.F. Wei ,S.J. Xu, W.K. Chan, *Chem. Phys. Lett*. **394**, 452 (2004)

[9] W.L. Zhou, J.B. He, J.Y. Fang, T.A. Huynh, T.J. Kennedy, K.L. Stokes, and C.J. O'Connor, *J. Appl. Phys.*, **93**,7340 (2003).

[10] J.J. Wu, and S.C. Liu, *J. Phys. Chem. B*, **106,** 9546 (2002).

[11] A.M. Morales, and C.M. Lieber, *Science*, **279**,208 (1998).

[12] W.I. Park, D.H. Kim, S.W. Jung, and G.C. Yi, *Appl. Phys. Lett.*, **80**,4232 (2002) .

[13] T.J. Trentler, K.M. Hickman, S.C. Goel, A.M. Viano, P.C. Gibbons, and W.E. Buhro, *Science*, **270**, 1791 (1995).

[14] Y. Li, G.W. Meng, L.D. Zhang, and F. Philipp, *Appl. Phys. Lett.*, **76**, 2011 (2000).

[15]M. Huang, S. Mao, H. Feick, H. Yan, Y. Wu, H. Kind, E. Weber, R. Russo, P. Yang, *Science*, **292**, 1897 (2001).

[16] X. F. Duan, Y. Huang and C.M. Lieber, *Nature*, **421**, 241 (2003).

[17] L. J. Lauhon, M. S. Gudiksen, D. Wang and C.M. Lieber, *Nature*, **420**, 57 (2002).

[18]Y. Huang, X.F. Duan, Y. Cui, L.J. Lauhon, K.H. Kim, and C.M. Lieber, *Science*, **294**, 1531 (2001).

[19]M. C. McAlpine, R. S. Friedman, S. Jin, K. H. Lin, W. U. Wang, and C.M. Lieber, *Nano Lett* , **3**, 1313 (2003).

[20]T. Yatsui, J. Lim, M. Ohtsu, S. J.An, G. C. Yi, *Appl. Phys. Lett.,* **85**, 727 (2004)

[21]M. H. Huang, S. Mao, H. Q. Yan, Y. Y. Wu, H. Kind, E. Webber, R. Russo, and P. D. Yang, *Science* **292**,1897 (2001).

[22]P. Yang, H. Yan, S. Mao, R. Russo, J. Johnson, R. Saykally, N. Morris, J.Pham, R. He, and H. J. Choi, *Adv. Funct. Mater.,* **12**, 323 (2002).

[23]C. H. Liu, J. A. Zapien, Y. Yao, X. M. Meng, C. S. Lee, S. S. Fan, Y. Lifshitz, and S. T. Lee, *Adv. Mater.,* **15**, 838 (2003).

[24] H. Kind, H. Yan, B. Messer, M . Law, and P. Yang, *Adv. Mater.,* **14**, 158 (2002).

[25]K. Keem, H. Kim, G. T. Kim, J. S. Lee, B. Min, K. Cho, M. Y. Sung, and S. Kim, *Appl. Phys. Lett.,* **84**, 4376 (2004).

[26] S. H. Dalal1, D. L. Baptista, K. B. K. Teo, R. G. Lacerda, D. A. Jefferson, and W. I. Milne, *Nanotechnology* **17** 4811－4818 (2006),*Nanotechnology,* **17**, 1046-1051 (2006).

[27] A. Colli, A. Fasoli1, S. Hofmann, C. Ducati, J. Robertson, and A. C. Ferrari1, *Nanotechnology,* **17,** 1046－1051 (2006).

Chapter 2 Theoretical background

2.1 Growth mechanism of ZnO nanostructures

Previous effort in synthesis of ZnO nanowires and nanorods have employed vapor-phase transport via a vapor-liquid-solid (VLS) mechanism [1, 2], vapor solid mechanism [3, 4], and oxidation of metal in pores of anodic alumina templates [5, 6]. In this research, the vapor-phase transport was used to grow the ZnO nanowires. Most popular fabrication of ZnO nanowires with single crystalline structure and large quantities is by the VLS method. The VLS method was originally developed by Wagner and his co-workers to produce micrometer-sized whisker in 1960s [7], and recently re-examined successfully by Lieber [8] and Yang [3, 4]. In the VLS method, the catalyst plays a key role on growth of nanowires or nanorods. The catalyst would form an alloy nanoclusters are supersaturated in the reactant. All of the major formation procedure of 1-D nanostructure involved in VLS process is schematically illustrated in Fig. 2-1. [9] The reactant metal vapor which could be generated by the thermal evaporation is condensed to the catalyst metal to form a liquid alloy nanocluster as the temperature is low. The liquid metal alloys become supersatured and continue as long as the metal nanoclusters remain in a liquid state before nanowires being grown. Growth of nanowires will be terminated as the temperature reduces to the point that the metal nanoclusters solidify. Therefore, a strong evidence of the VSL mechanism is to observe catalytic metal at the end of the nanowires as that observes on the formation of Ge nanowire in the report by P. Yang *et al*. [9], as shown in Fig. 2-2.
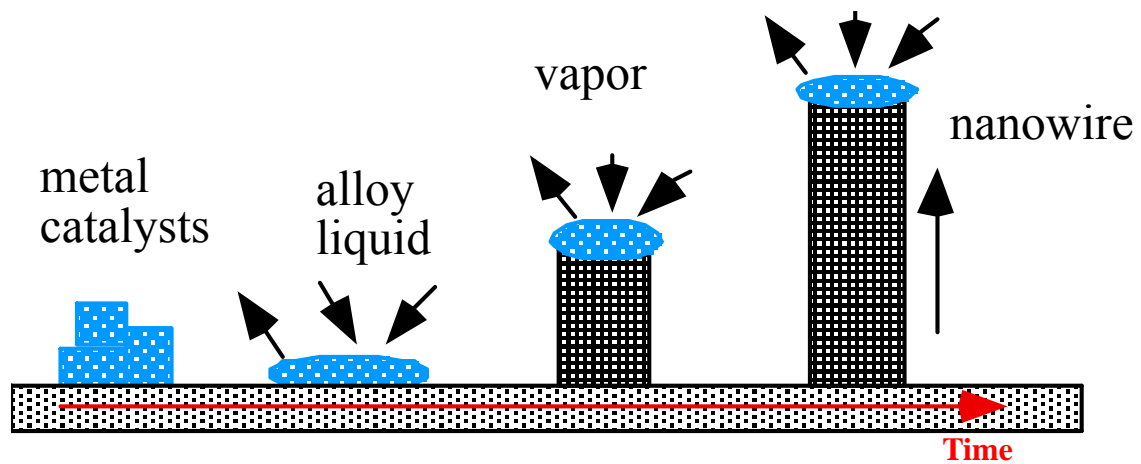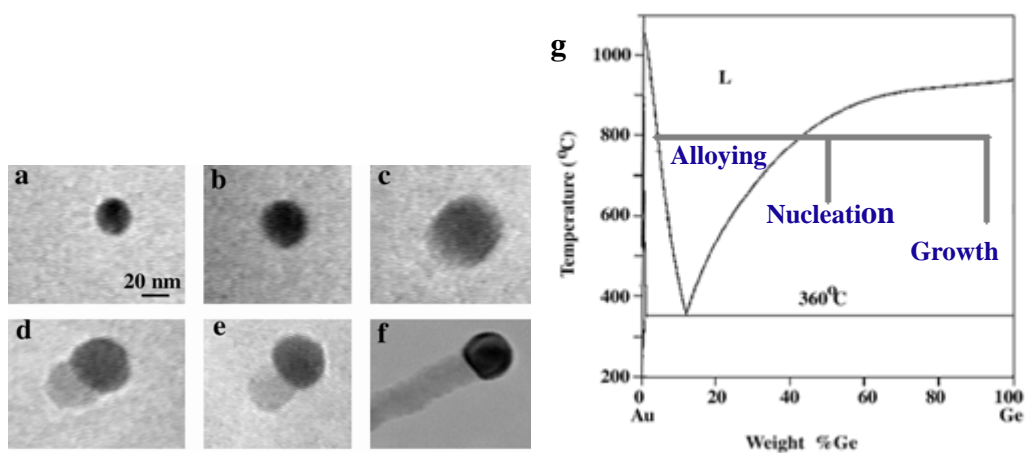
Fig. 2-1 VLS method

Fig. 2-2 In situ TEM images recorded during the process of nanowire growth.　(a) Au nanoclusters in solid state at 500 C; (b) Alloying is initiated at 800 ^{o}C, at this stage Au exists mostly in solid state; (c) liquid Au/Ge alloy; (d) the nucleation of a Ge nanocrystal on the alloy surface; (e) Ge nanocrystal elongates with further Ge condensation; (f) eventually forms a wire; and (g) Au-Ge binary phase diagram. [9]

2.2 Scanning Electron Microscope (SEM)

The principle of SEM used for examining a solid specimen in the emissive mode is closely comparable to that of a closed circuit TV system shown in Fig. 2-3.　In the TV camera, light emitted from an object forms an image on a special screen, and the signal from the screen depends on the intensity of image at the point being scanned. The signal is used to modulate the brightness of a cathode ray tube (CRT) display, and the original image is faithfully reproduced if (a) the camera and display raster are

geometrically similar and exactly in time and (b) the time for signal collection and processing is short compared with the time for the scan moving from one picture point to the next.

In the SEM the object itself is scanned with the electron beam and the electrons emitted from the surface are collected and amplified to form the video signal. The emission varies from point to point on the specimen surface, and so an image is obtained. Many different specimen properties cause variations in electron emission, thus, although information might be obtained about all these properties, the images need interpreting with care. The resolving power of the instrument can not be smaller than the diameter of the electron probe scanning across the specimen surface, and a small probe is obtained by the demagnification of the image of an electron source by means of electron lenses. The lenses are probe forming rather than image forming, and the magnification of the SEM image is determined by the ratio of the sizes of raster scanned on the specimen surface and on the display screen. For example, if the image on the CRT screen is 100 mm across, magnifications of 100X and 10000X are obtained by scanning areas on the specimen surface 1mm and $10\mu m$ across, respectively. One consequence is that high magnifications are easy to obtain with the SEM, while very low magnifications are difficult. This is because large angle deflections are required which imply wide bore scan coils and other problem parts, and it is more difficult to maintain scan linearity, spot focus and efficient electron collection at the extremes of the scan.
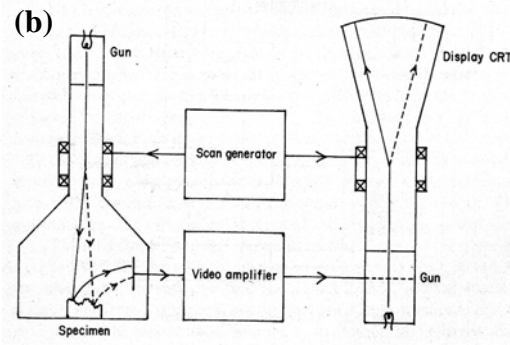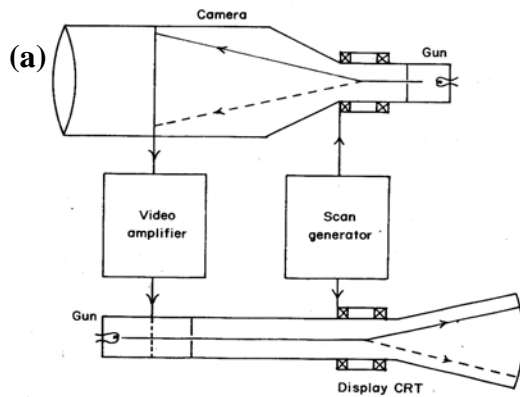
Fig.2-3 (a) Closed circuit TV and (b) scanning electron microscope

2.3 X-ray diffraction [10, 11]

A crystal consists of orderly array of atoms, each of which can scatter electromagnetic waves. A monochromatic beam of X-rays that falls upon a crystal will be scattered in all directions inside it. However, owing to the regular arrangement of the atoms, in certain directions the scattered waves will constructively interfere with one another while in others they will destructively interfere. The peaks of an x-ray diffraction pattern are made up of constructively interfere with planes, this analysis was suggested in 1913 by W. L. Bragg. Consider an incident mono chromatic x-ray beam interacting with the atoms arranged in a periodic manner as show in 2-dimendion in Fig. 2-4. The atoms, represented as circles in the graph forming different sets of plane in the crystal. To give a set of lattice planes with an inter-plane distance of d, the condition for diffraction (peak) constructively interfere to occur can be simply written as

$$2d \sin \theta = n\lambda , \qquad n = 1,2,3,... \qquad (2.1)$$

which is known as the Bragg's law. In this equation, λ is the wavelength of the x-ray, θ is the diffraction angle, and *n is* an integer representing the order of the diffraction peak.
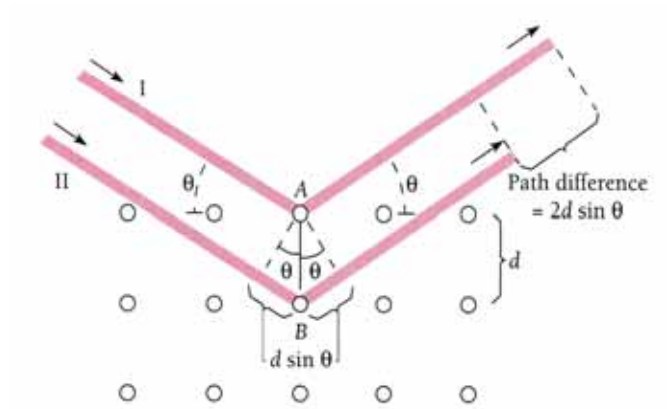
Fig. 2-4 x-ray scattering from a 2-dimendion periodic crystal

Considering hexagonal unit cell which is characterized by lattice parameters a and c. The plane spacing equation for hexagonal structure is

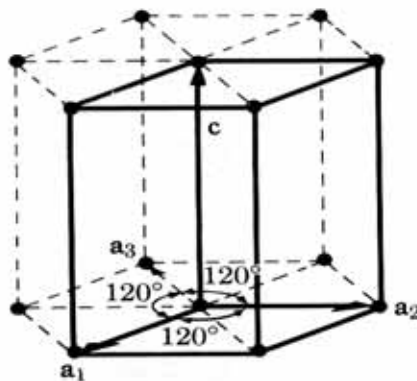$$\frac{1}{d^2} = \frac{4}{3}\left(\frac{h^2 + hk + k^2}{a^2}\right) + \frac{l^2}{c^2}. \tag{2.2}$$

Combining Bragg's law ($\lambda = 2d\sin\theta$) with (2-2) yields:

$$\frac{1}{d^2} = \frac{4}{3}\left(\frac{h^2 + hk + k^2}{a^2}\right) + \frac{l^2}{c^2} = \frac{4\sin^2\theta}{\lambda^2}. \tag{2-3}$$

Rearranging (2-3) gives

$$\sin^2\theta = \frac{\lambda^2}{4}\{\frac{4}{3}\left(\frac{h^2 + hk + k^2}{a^2}\right) + \frac{l^2}{c^2}\}, \tag{2-4}$$

Thus the lattice parameters can be estimated from Eq. 2-5.

13

Fig. 2-5 The hexagonal unit cell

2.4 Raman scattering

When the light encounters the medium, the light is reflected, transmitted, absorbed, elastic scattered, or inelastic scattered. Raman scattering is an inelastic scattering process. When light passes through a medium, it interacts inelastically with phonons and produces an outgoing photon whose frequency is relatively shifted by an amount of energy corresponding to phonon energy from that of the incoming light. That scattered outgoing photon call the Raman-scattered photons. Raman scattering is inherently a weak process, but laser provides enough intensity that the spectra can be routinely measured. In analogy with terms used in the discussion of fluorescence spectra, lines on the low frequency side of the excitation line are known as the Stokes lines and those on the high frequency side as the anti-Stokes lines. They gain energy by absorbing a phonon (anti-Stokes shift), or lose energy by emitting a phonon (Stokes shift), according to the energy and momentum conservation rules:

$$h\nu_s = h\nu_i \pm h\Omega$$
$$q_s = q_i \pm K$$
(2.18)

where ν_i and ν_s are the incoming and scattered photon frequencies, q_i and q_s are the incoming and scattered photon wavevectors, and Ω and K are the phonon frequency and wavevector, respectively.

All of the Raman mode intensities, frequencies, line-shapes, and line-widths, as well as polarizations can be used to characterize the lattices and impurities. The intensity gives information on crystallinity. The line-width increases when a material is damaged or disordered, because damage or disorder occurs in a material will add phonon damping rate or relax the rules for momentum conservation in Raman process. All these capabilities can be used as a judgment for layered

14

microstructures as well as bulk materials, subject only to the limitation that the penetration depth of the excitation radiation range from a few hundred nanometers to few micrometers.

The E_2 mode of the wurtzite ZnO crystal would shift to a higher frequency under the biaxial compressive stress within the c-axis oriented ZnO by the equation:

$$\Delta\omega(cm^{-1}) = 4.4\sigma(GPa) \,, \tag{2-19}$$

where $\Delta\omega$ is the frequency shift, and σ is the stress in the biaxial direction of lattice.

2.5 Photoluminescence Characterization [12,13]

Photoluminescence (PL) is a very powerful optical tool for the semiconductor industry, with its sensitivity to find the emission mechanism and band structure of semiconductors.   From PL spectrum the defect or impurity can also be found in the compound semiconductors, which affect material quality and device performance.   A given impurity produces a set of characteristic spectral features.   The fingerprint identifies the impurity type, and often several different impurities can be seen in a single PL spectrum.   In addition, using the PL peak their full width of half width is an indication of sample's quality, although such analysis has not yet become highly quantitative. [14]

PL is the optical radiation emitted by a physical system (in excess the thermal equilibrium blackbody radiation) resulting from excitation to a nonequilibrium state by illuminating with light.   Three processes can be distinguished: (i) creation of electron-hole pairs by absorption of the excited light, (ii) radiative recombination of electron-hole pairs, and (iii) escape of the recombination radiation from the sample.

2.5.1 Fundamental Transitions

The absorption of a photon by an interband transition in a semiconductor creates an electron in the conduction band and a hole in the valence band. The oppositely charged particles are created at the same point in space and can attract each other through their Coulmb interaction. This attractive interaction increases the probability of formation of an electron-hole pair, and therefore, increases the optical transition rate. We will consider the fundamental transitions, those occurring at or near the band edges.

1. Free excitons (Wannier-Mott excitons)

A free hole and a free electron as a pair of opposite charges experience a coulomb attraction. The type excitons have a large radius that encompasses many atoms, and they are delocalized states that can move freely throughout the crystal; hence the alternative name of free excitons. If the material is sufficiently pure, the electrons and holes pair into excitons which then recombine, emitting a narrow spectral line. In a direct-gap semiconductor, where momentum is conserved in a simple radiative transition, the energy of the emitted photon is simply $h\nu=E_g - E_b$, where E_g and E_b are the band gap and the exciton binding energy. We can calculate the emission photon energy by hydrogen-like atom model.

$$E_{ph}=E_g-R_{y(}\frac{1}{n^2}) + \frac{\hbar^2 K^2}{2M},$$ (2.20)

where n=1,2,3,... is the principle number, $R_y=13.6(\frac{\mu}{m_0 \varepsilon^2})$ is exciton binding energy, M=m_e + m_h, and K = k_e + k_h are translational mass and wave vector of the exciton, respectively.

2. Bound excitons

Similar to the way that free carriers can be bound to defects, it is found that excitons can also be bound to defects. A free hole can combine with a neutral donor to form a positively charged excitonic ion. In this case, the electron bound to the donor still travels in a wide orbit about the donor. The associated hole moves in the electrostatic field of the "fixed" dipole, determined by the instantaneous position of the electron, then also travels about this donor; for this reason, this complex is called a "bound exciton". An electron associated with a neutral acceptor is also a bound exciton. The binding energy of an exciton to a neutral donor (acceptor) is usually much smaller than the binding energy of an electron (hole) to the donor (acceptor).

3. Donor-Acceptor Pairs (DAP)

Donors and acceptors can form pairs and act as stationary molecules imbedded in the host crystal. The coulomb interaction between a donor and an acceptor results in a lowering of their binding energies. In the donor-acceptor pair case it is convenient to consider only the separation between the donor and the acceptor level:

$$E_{pair} = E_g - (E_D + E_A) + \frac{q^2}{\varepsilon \ r} \ , \qquad\qquad (2\text{-}21)$$

where r is the donor-acceptor pair separation, E_D and E_A are the respective ionization energies of the donor and the acceptor as isolated impurities.

4. Deep transitions

By deep transition we shall mean either the transition of an electron from the conduction band to an acceptor state or a transition from a donor to the valence band in Fig. 2-9. Such transition emits a photon $h\nu = E_g - E_i$ for direct transition and $h\nu = E_g - E_i - E_p$ if the transition is indirect and involves a phonon of energy E_p. Hence the deep transitions can be distinguished as (I) conduction-band-to-acceptor

transition which produces an emission peak at $h\nu = E_g - E_A$, and (Ⅱ) donor-to-valence-band transition which produces emission peak at the higher photon energy $h\nu = E_g - E_D$.
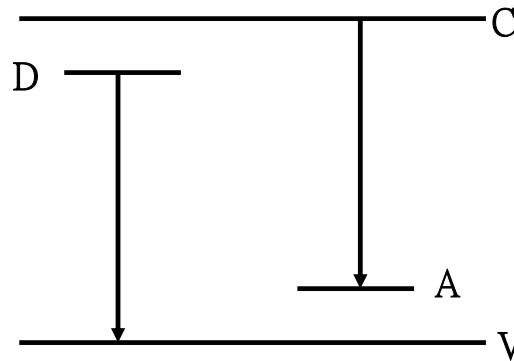

Fig. 2-6 Radiative transition between a band and an impurity state

2.5.2 Influence of high excited light intensity

The PL conditions as mentioned above are excited by low excitation light intensity. At low excitation light intensity (low density regime in Fig. 2-7), the PL properties are determined by single electron-hole pairs, either in the exciton states or in the continuum. Higher excitation intensity (intermediate density regime in Fig. 2-7) makes more excitons; such condition would lead to the exciton inelastic scattering processes and form the biexciton. The scattering processes may lead to a collision-broadening of the exciton resonances and to the appearance of new luminescence bands, to an excitation-induced increase of absorption, to bleaching or to optical amplification, i.e., to gain or negative absorption depending on the excitation conditions. If we pump the sample even harder, we leave the intermediate and arrive at the high density regime in Fig. 2-7, where the excitons lose their identity as individual quasiparticles and where a new collective phase is formed which is known as the electron-hole plasma (EHP).
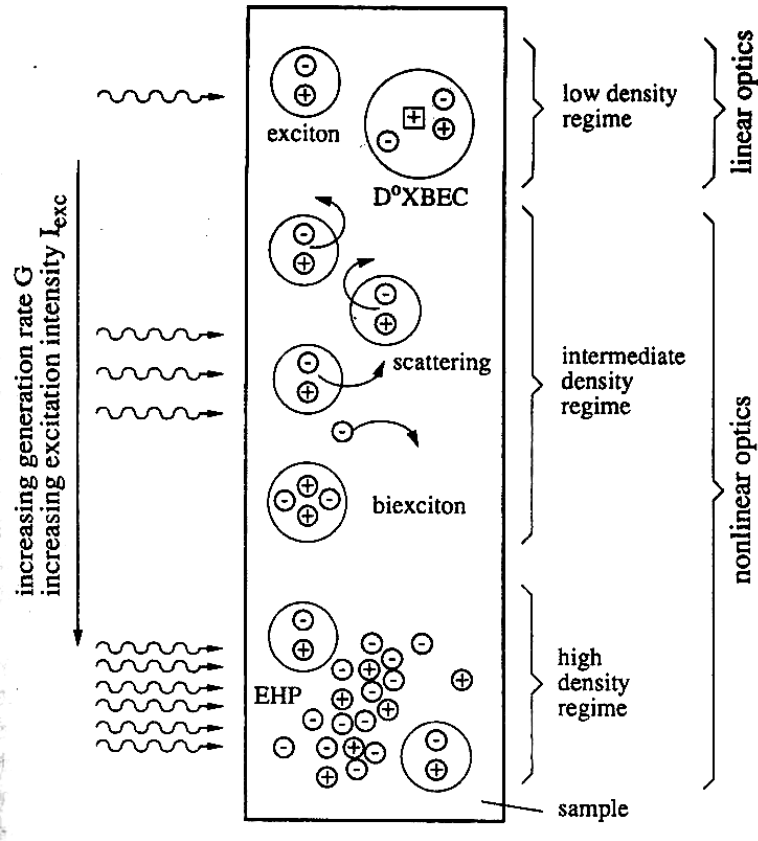
Fig. 2-7 The general scenario for many-particle effects in semiconductors. [13]

1.   Electron-Hole Plasma

In this high density regime, the density of electron-hole pairs n_p is at least in parts of the excited volume so high that their average distance is comparable to or smaller than their Bohr radius, i.e., we reach a "critical density" n_p^c in an EHP, given to a first approximation by $a_B^3 n_p^c \approx 1$. We can no longer say that a certain electron is bound to a certain hole; instead, we have the new collective EHP phase. The transition to an EHP is connected with very strong changes of the electronic excitations and the optical properties of semiconductors.

2.   Scattering Processes

In the inelastic scattering processes, an exciton is scattered into a higher excited state, while another is scattered on the photon-like part of the polariton dispersion and leaves the sample with high probability as a luminescence photon,

when this photon-like particle hits the surface of the sample.   This process is shown

schematically in Fig. 2-8 and the photons emit in such a process have energies E_n

given by Ref. [15]

$$E_n = E_{ex} - E_b^{ex}\left(1 - \frac{1}{n^2}\right) - \frac{3}{2}kT ,\qquad\qquad (2\text{-}22)$$

where n = 2, 3, 4,…, E_b^{ex} =60meV is the binding energy of the free exciton of ZnO,

and kT is the thermal energy.   The resulting emission bands are usually called
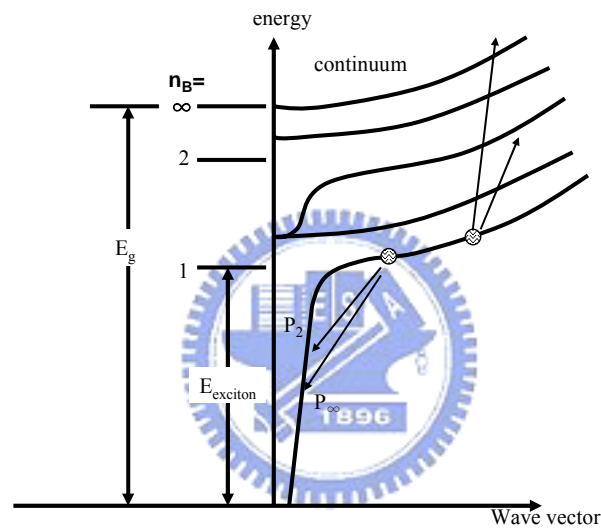
P-bands with an index given by n.

Fig.2-8 Schematic representation of the inelastic exciton-exciton scattering processes. [13]

References

[1] M. H. Huang, Y. Wu, H. Feick, N. Tran, E. Weber and P. D. Yang. *Adv. Mater.,* **13**, 113 (2001).

[2] M. H. Huang, S. Mao, H. Feick, Y. Wu, H. Kind, E. Weber, R. Russo and P. D.Yang. *Science,* **292**, 1897 (2001).

[3] Z. W. Pan, Z. R. Dai and Z. L. Wang, *Science,* **291**, 1947 (2001).

[4] J. Q. Hu, Q. Li, N. B. Wong, C. S. Lee, and S.T. Lee, *Chem. Matter.,* **14**, 1216 (2002).

[5]Y. Li, G. W. Meng, L. D. Zhange, F. Phillipp, *Appl. Phys. Lett.*, **76**, 2011 (2000).

[6] C. H. Liu, J. A. Zapien, Y. Yao, X. M. Meng, C. S. Lee, S. S. Fan, Y. Lifshitz, and S. T. Lee, *Adv. Mater.,* **15**, 838 (2003).

[7]R. S. Wagner, and W. C. Ellis, *Appl. Phys. Lett.,* **4**, 89 (1964).

[8]A. M. Morales, and C. M. Lieber., *Science,* **279**, 208. (1998).

[9] Y. Wu, and P. Yamg. *J. Am. Chem. Soc.,* **123**, 3165 (2001).

[10] B. D. Cullity, Element of X-ray diffraction, 2 nd ed, (Addison Wesley, Canada 1978).

[11] A. Taylor: X-ray Metallography (John Wiley and Sons, New York, 1961).

[12] F. Mark, Optical Properties of Solids (Oxfrd university press).

[13] C. F. Klingshirn, Semiconductor Optics (Springer, Berlin).

[14] Sidney Perlpwotz, *Optical characterization of semiconductors: infaraed, Raman, and Pholuminescence spectroscopy,* (Academic Press, London, 1993) p.61.

[15] J.B. Baxter, E.S. Aydil, *Appl. Phys. Lett.,* **86,** 053114-1 (2005).

Chapter 3 Experiment Details

3.1 Sample Preparation

3.1.1 Substrate preparation

The *a*-plane sapphires were used as the substrate for the growth of ZnO nanostructures.　Before the surface treatment, the substrates were cut into an area of 10×5 mm^2 for the nanostructures growth.　Then these substrates were cleaned by using the following steps:

　　(1) Rinsed in D. I. water by a supersonic oscillator in 10 min.

　　(2) Rinsed in ACE (Acetone) solution by a supersonic oscillator in 5 min.

　　(3) Rinsed in D.I water by a supersonic oscillator in 10 min.

　　(4) Rinsed in H_2O_2 + H_2SO_4 (1:3) solution by a supersonic oscillator 10min

　　(5) Repeat (3).

　　(6) Dried with N_2 gas.
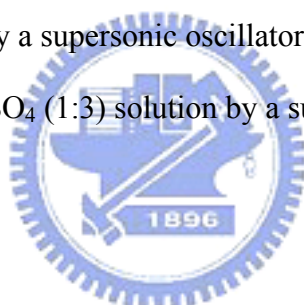
After the surface treatment, the substrates were placed in an alumina boat ready to grow ZnO nanostructures.

3.1.2 Growth of ZnO nanostructures

1.　Conventional VS method

The alumina boat which carried the substrate and pure Zn powder together was inserted into a quartz tube.　This quartz tube was placed inside a furnace that is 65 cm long.　The alumina boat positioned that placed the substrate and Zn powder at the center of the furnace.　The quartz tube was evacuated to a pressure below ≈ 50 torr using a mechanical pump, then, the high-purity argon gas was infused into the system with a flow rate of 500 sccm.　The temperature of the furnace was increased to

540^0C at a rate of 30^0C min^{-1} to grow ZnO nanowires without preheating the substrate. The furnace was cooled to room temperature at the rate of 10 ^{0}C /min.

2. Modified VS method

We modified the conventional VS method by using two alumina boats to separately carry the substrate and Zn powder (99.9999 %).   First of all, the alumina boat that carried substrate was placed at the center of the furnace and left the Zn-source boat outside the furnace (Fig. 3-1).   After the quartz tube had been evacuated to a pressure below $\approx 10^1$ torr using a mechanical pump, high-purity argon gas was then infused into the system with a flow rate of 500 sccm.   The temperature of the furnace was raised to 460^0C~580^0C at a rate of 30^0C/min and kept at the target temperature for 20 min to heat up the substrate.   Secondly, the Zn-source boat was pushed inside the furnace and kept against the substrate boat at the target temperature for another 80 min to grow ZnO nanowires.   After the growth procedure has completed, the furnace was cooled at 10^0C/min to the room temperature.   Dark gray-white material was obtained on the surface of the substrate.
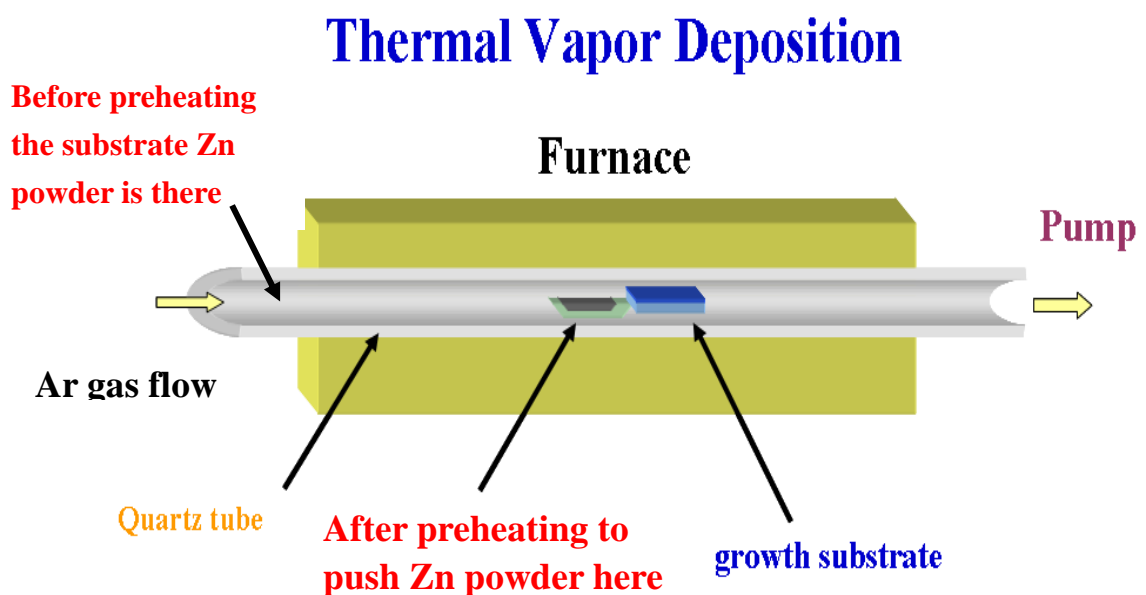

Fig. 3-1 Thermal vapor transport system

3.2 Structure analysis: SEM and XRD

3.2.1 Scanning Electron Microscope

The morphology of ZnO-based nanostructures was observed by the Field Emission Scanning Electron Microscopy (FESEM) [HITACHI S-4000] as shown Fig. 3-2.   The accelerated voltage and emission extracting voltage is 0.5-30 kV and 0 ~ 6.5 kV, respectively, and the magnification is 20-300k times so that the best resolution is 1.5 nm at 25 keV.   The sample holder of FESEM can be tuned at an angle of 45^0 to take side view.
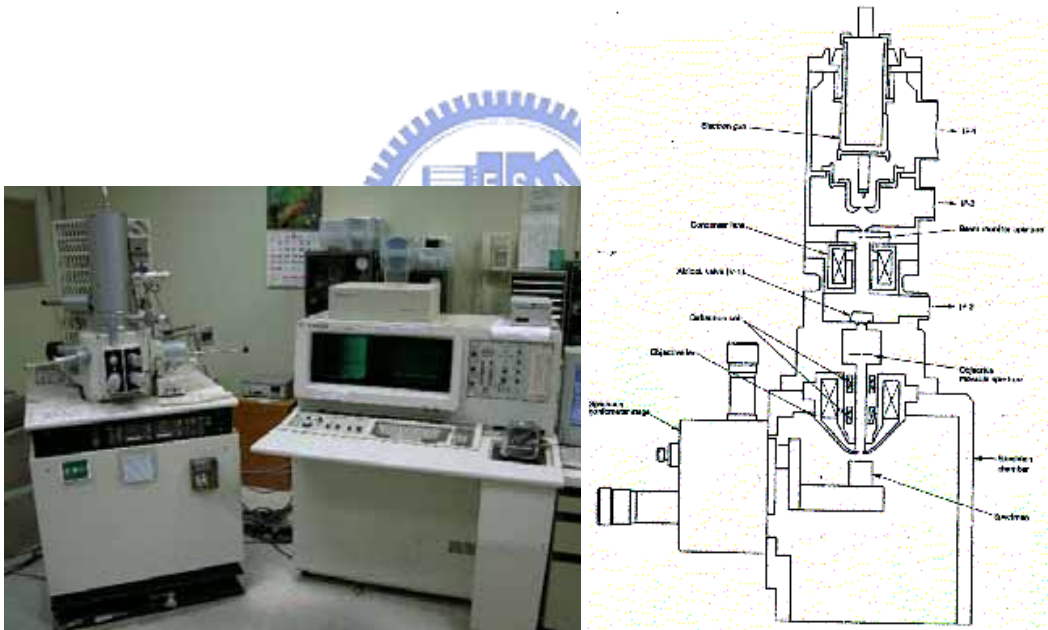

Fig. 3-2 FESEM system.

3.2.2 X-ray diffraction

After growing the nanostructures, the crystalline structures of the as-grown ZnO nanowires were analyzed by using Philips PW1700 X-ray diffractometer (XRD) with Cu Ka_1 radiation (λ=1.5405 Å).   The maximum voltage of the system is 40 kV with

a maximum current 40 mA.　The sampling width is 0.020^{o} and scanning rate is 40 degree/min.

3.3 Optical property: Raman and PL spectroscopies

3.3.1 Raman system

The optical characterization was analyzed with Raman spectroscopy.　A 20mW Ar-ion laser with an incident wavelength of 488 nm was used as the excitation source for the Raman spectroscopy.　The scattered light was collected using backscattering geometry and detected by the SPEX 1877 triplemate equipped with liquid nitrogen cooled CCD.　Measurements were carried out at room temperature, as shown in Fig. 3-3.
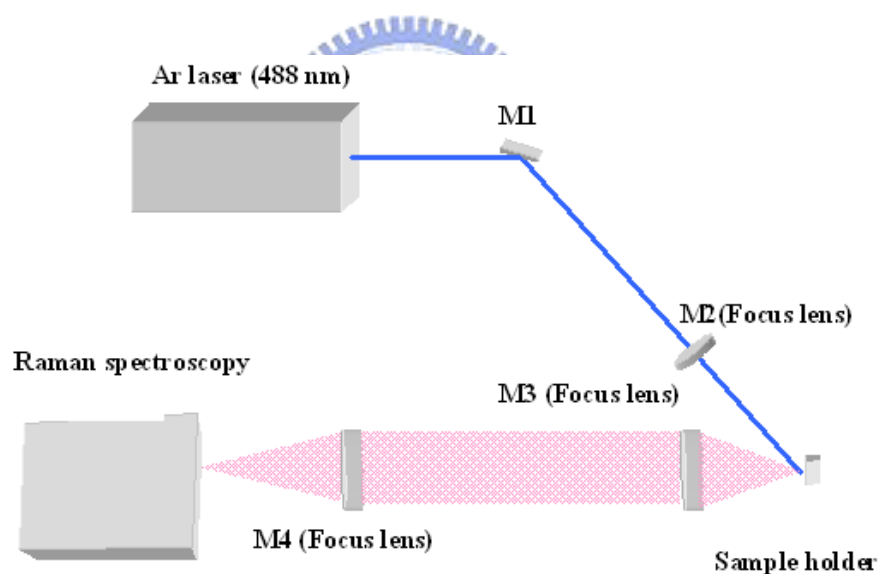

Fig. 3-3 Raman system.

3.3.2 Photoluminescence (PL) system

For PL measurement, we used a He–Cd cw laser (325 nm) [Kimmon IK5552R-F] as the excitation source.　The emission light was dispersed by a TRIAX-320 spectrometer and detected by a UV-sensitive photomultiplier tube, as shown in Fig.
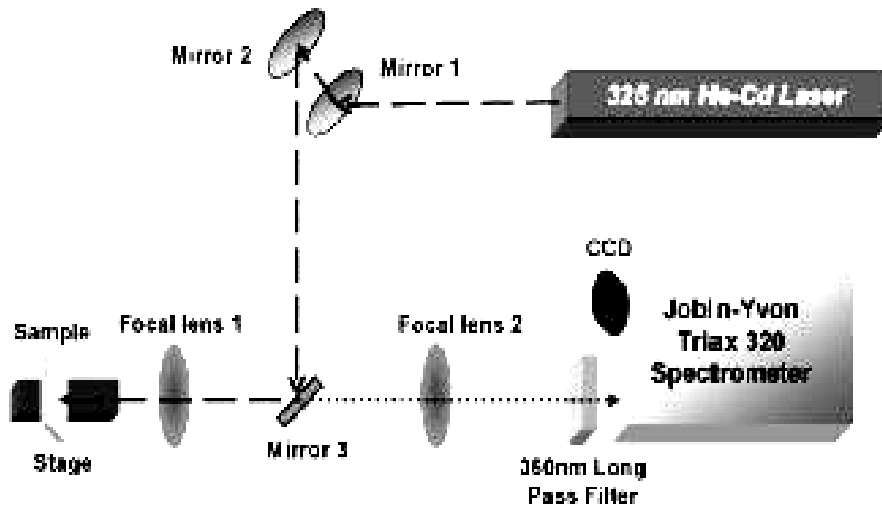
3-4.

Fig. 3-4 The PL system

Chapter 4 Results and Discussion

4.1 Structural properties of ZnO nanowires

4.1.1 Growth of ZnO nanowires on α-sapphire

In recent report deterministic shape-selective synthesis of nanostructures [1], controlled the temperature of substrate and compound source temperature used preheated substrate and using pressure shutter. Using the same idea, if substrate is preheated to the target temperature before introducing the Zn source, we may be able to deterministic synthesize single mprphology ZnO nanowires. We used sapphire $(11\bar{2}0)$ wafer as the substrate to grow ZnO nanowires by simple vapor transport deposition. Two ceramic boats prepare for placing the substrate and 1g pure Zn powder (99.999%) as the starting materials. After the high-purity argon gas was infused into the system with a flow rate of 500 sccm, the furnace temperature was increased to near 550 ℃ and kept at this temperature for 20 min to preheating the substrate. Then the source boat was pushed into the center of furnace to growth ZnO nanowires, the temperature of the furnace was still fixed near 550 ℃ for 80 min. After the reaction is complete, the system was cooled to the ambient temperature and a gray-white colored product was found deposited on the substrate.

4.1.2 Structural properties and growth mechanism of ZnO nanowire

As shown in Fig. 4-1(a) and (b), the typical SEM micrographs of samples grown by conventional VS (sample a) and modified VS (sample b) methods, respectively that clearly reveal a large quantity of nanowires were formed on α-plane the sapphire $(11\bar{2}0)$ substrate.

High magnification oblique view and cross-section images were shown in Fig.

4-1(c) and (d) and Fig. 4-1(e) and (f) individually. Typical length of nanowires exceeds 1μm and diameter of about 120 nm. The thickness of the ZnO buffer layer grown by the modified VS method is less than 50 nm and that grown by the conventional VS method is larger than 2 μm. Furthermore, it seems that each one of the wires is grown from a single individual grain on the buffer layer for the sample (b); but the sample (a) seems to have smoother and thicker buffer layer. This difference should reflect on the grown texture of the nanowires.
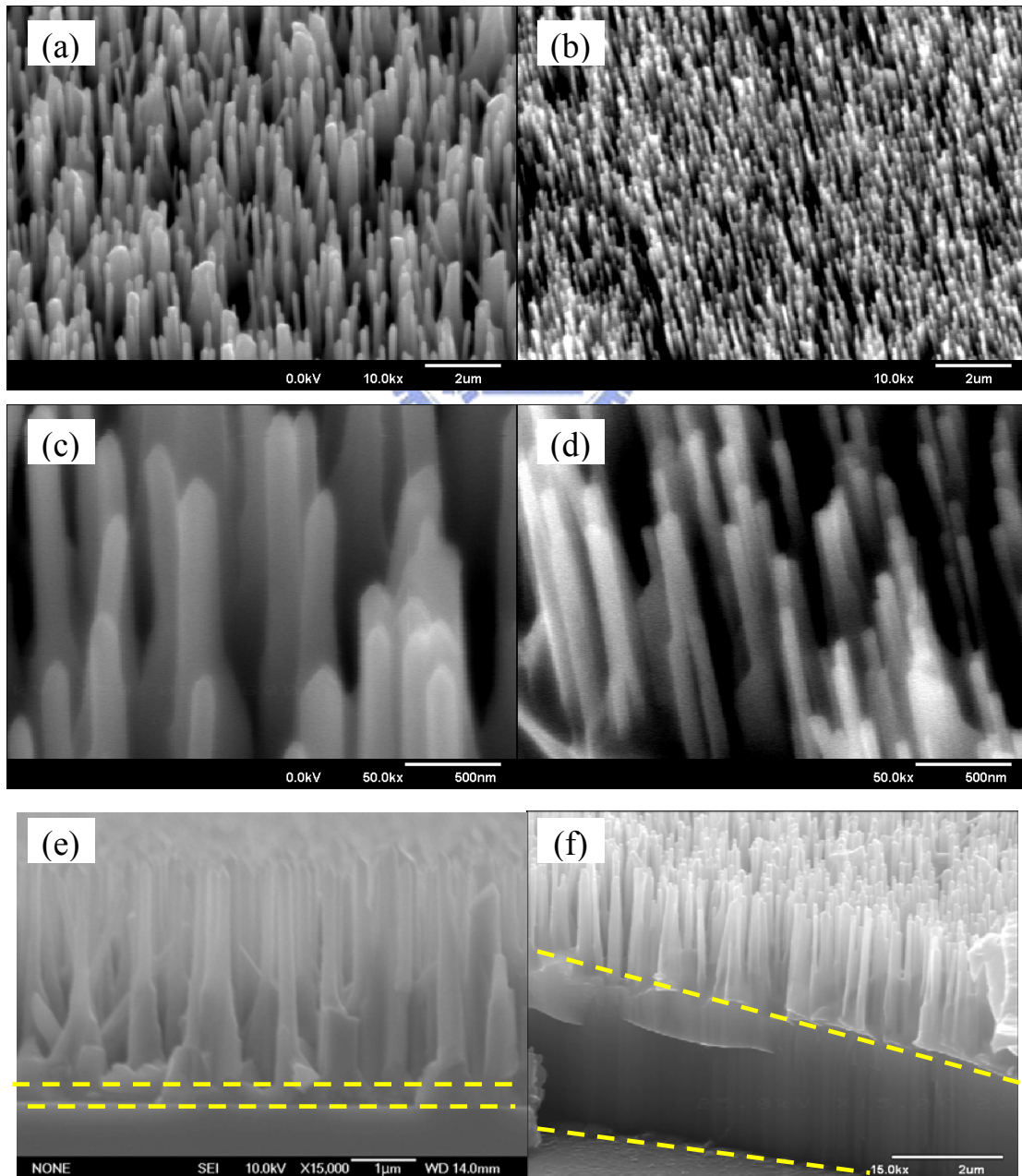
Fig. 4-1 The oblique and cross section views of SEM images of ZnO nanowires grown by the modified

VS and the conventional VS methods.　(a) and (b) are the SEM oblique images of ZnO

nanowires; (c) and (d) the magnified oblique view images of the ZnO nanowires; (e) and (f)

the cross sections of the ZnO nanowires.　Note that (a), (c) and (e) are for the sample

grown by the modified VS method, whereas, (b), (d), and (f) for that grown by the

conventional VS method.

Figure 4-2 (a) and (b) show the XRD diffraction patterns of the samples shown in Fig. 4-1.　Besides the preferential (002) growth direction, a minor peak (101) peak can be found for the ZnO nanowires grown by the modified VS method.　The lattice constants calculated according to the following equations based on the wurtzite structure are a=3.245 Å and c=5.209 Å for sample (a) and a=3.250 Å and c=5.209 Å for sample (b):

$$a = \frac{\lambda}{2\sin\theta}\sqrt{\frac{4}{3}(h^2 + hk + k^2) + \frac{l^2}{(c/a)^2}} \qquad (4\text{-}1)$$

$$c = \frac{\lambda}{2\sin\theta}\sqrt{\frac{4}{3(c/a)^2}(h^2 + hk + k^2) + l^2} \; , \qquad (4\text{-}2)$$

where h, k, l are Miller exponents, and λ=1.54056Å and θ are X-ray wavelength and Bragg angle, respectively.

(a)

(002)

sapphire(110)

intensity (a.u.)

2θ (degree)

(b)

(002)

(101)

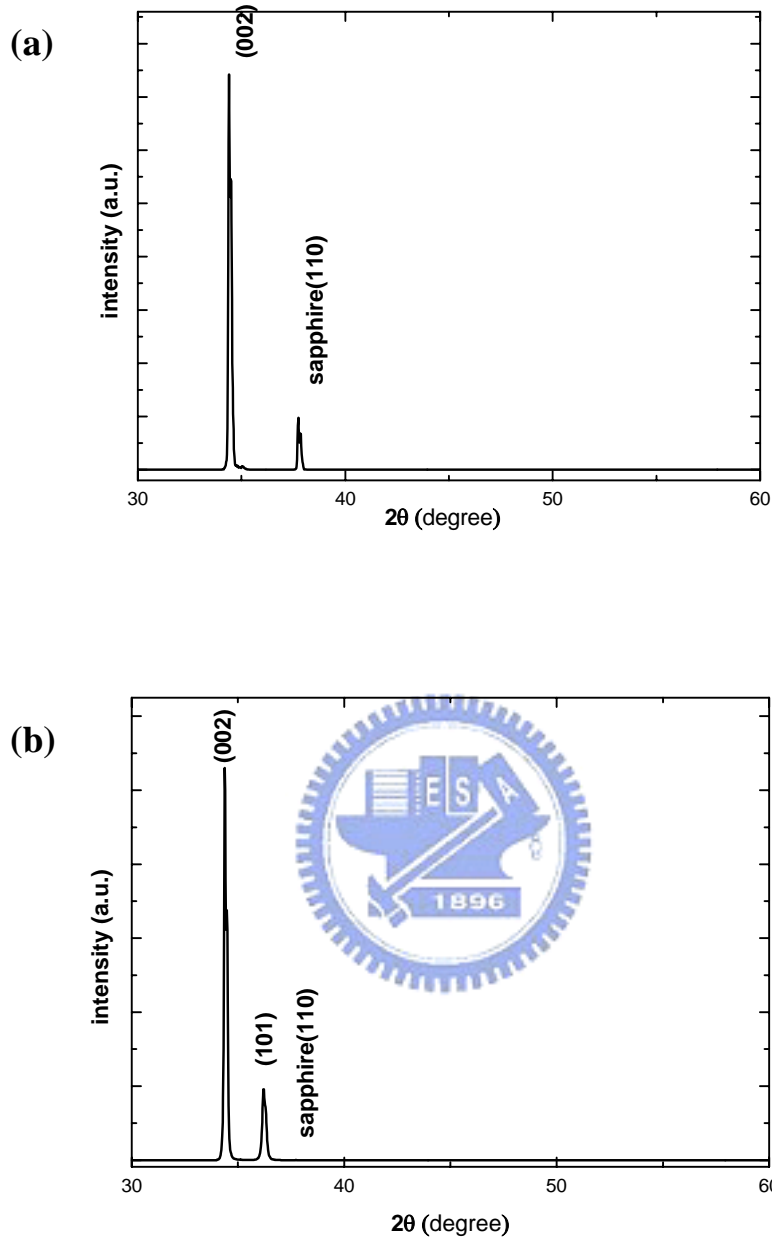sapphire(110)

intensity (a.u.)

2θ (degree)

Fig. 4-2 The XRD pattern of ZnO nanowires produced by the conventional VS method (a) and the modified VS method (b), respectively.

We further used the texture coefficient $T_{c(hkl)}$ [3] to evaluate the degree of preferential orientation of nanowires:

$$T_{c(hkl)} = \frac{I_{(hkl)}/I_{0(hki)}}{\frac{1}{N}\sum_{N}(\frac{I_{(hkl)}}{I_{0(hki)}})} ,$$
(4-3)

where $T_{c(hkl)}$ is the texture coefficient of (h k l) plane, I is the measured intensity, I_0 is the corresponding standard data (JCPDS 36-1451) intensity, N is the number of preferred growth directions. We obtained $T_{c(002)}$ and $T_{c(101)}$ to be 2.998 (99.93%) and 0.002 (0.07%) for the sample (a) that shows excellent (002) plane preference, so the conventional VS method tends to grow [002] prefer-oriented ZnO nanowires. On the other hand, the texture coefficient $T_{c(002)}$ and $T_{c(101)}$ calculated from the sample (a) are 2.803 (93.44%) and 0.197 (6.56%) that shows almost ZnO nanowire prefer to grow on [002] direction but with 6.5% grown along [101] direction. It may be attributed to the nanowires of the sample (b) almost all grow from island-like grains on the rough and thin buffer layer that [002] direction is not always perpendicular to the surface of a-plane sapphire substrate and the tip shape of some nanowires that the lateral faces of taper is in front of the tip be dominant (101) face. [20]

The growth mechanism of the nanowires is likely the self-catalyst process, which originates from Zn or ZnO_x clusters [4]. The possible growth procedure for typical ZnO nanowires is as follow. The Zn powder turns into Zn vapor during the evaporation duration and forms Zn or ZnO_x liquid droplets at the nucleation sites on the substrate. Then the solid ZnO particles form and separate from the droplets. As the reaction process proceeded with more Zn vapor turned into Zn or ZnO_x liquid droplets, and deposited on the more nucleation sites to form ZnO buffer layer. Finally, it is known that [002] is the fastest growth direction in the only grew along one side of ZnO nanostructures, including the nanowire [3-7]. By modified VS

method preheating the sapphire arrived at higher temperature that suit to grow wires structure to avoid deposition exceeding ZnO buffer layer, and we reduce the buffer layer and grow vertical ZnO nanowires successfully.

4.1.3 Growth temperature dependence on structural properties of ZnO nanowire by modified VS method

We have shown that it is possible to reduce the pre-growth buffer layer by using the modified VS method to grow ZnO nanostructure and to obtain deterministic shape synthesis of ZnO nanostructure [8].　We therefore, kept constant carrier Ar-gas, flow rate of 500 sccm and used different furnace temperatures at 460, 500, 520, 540 and 580 ℃, respectively, to grow ZnO nanostructures.　The results are shown in Fig. 4-3 (a) to (i).
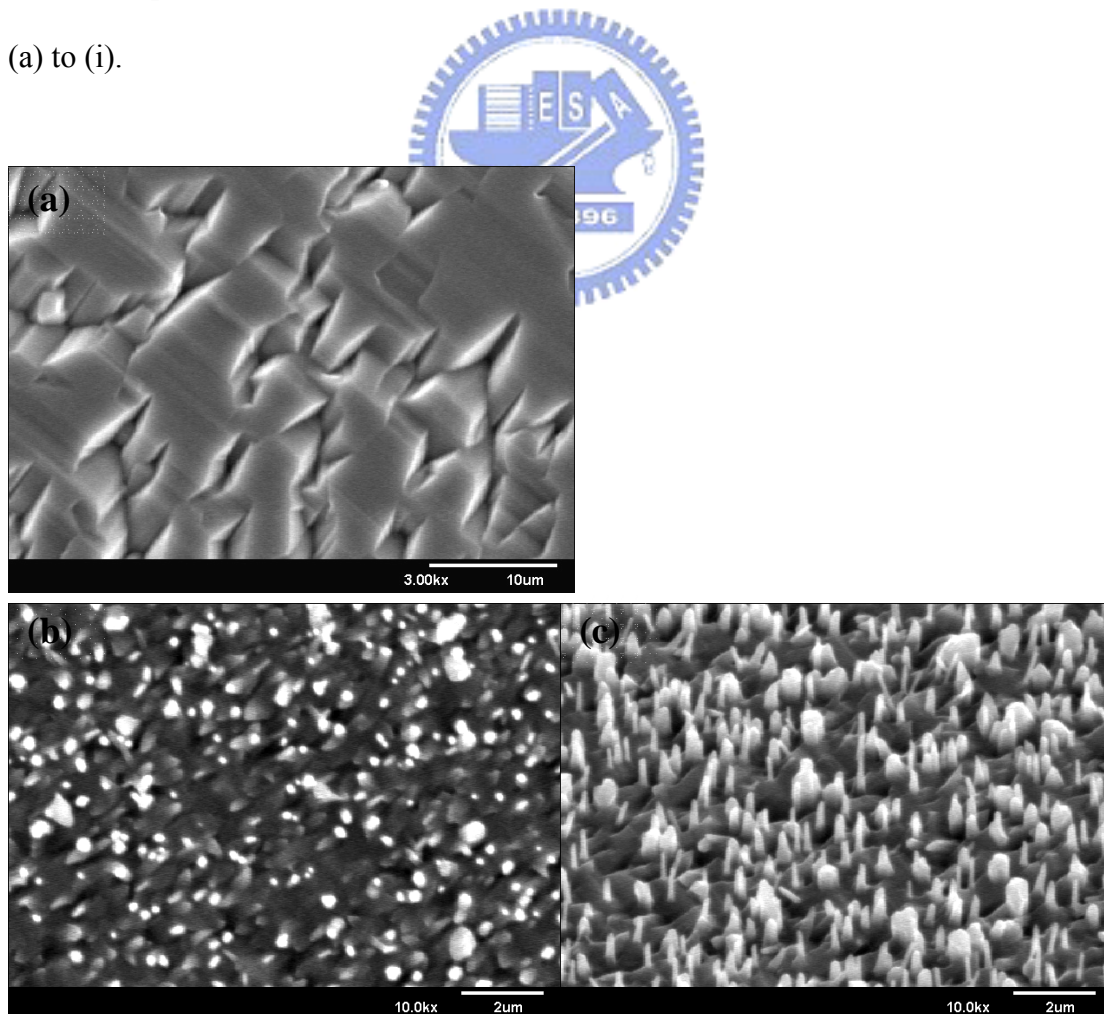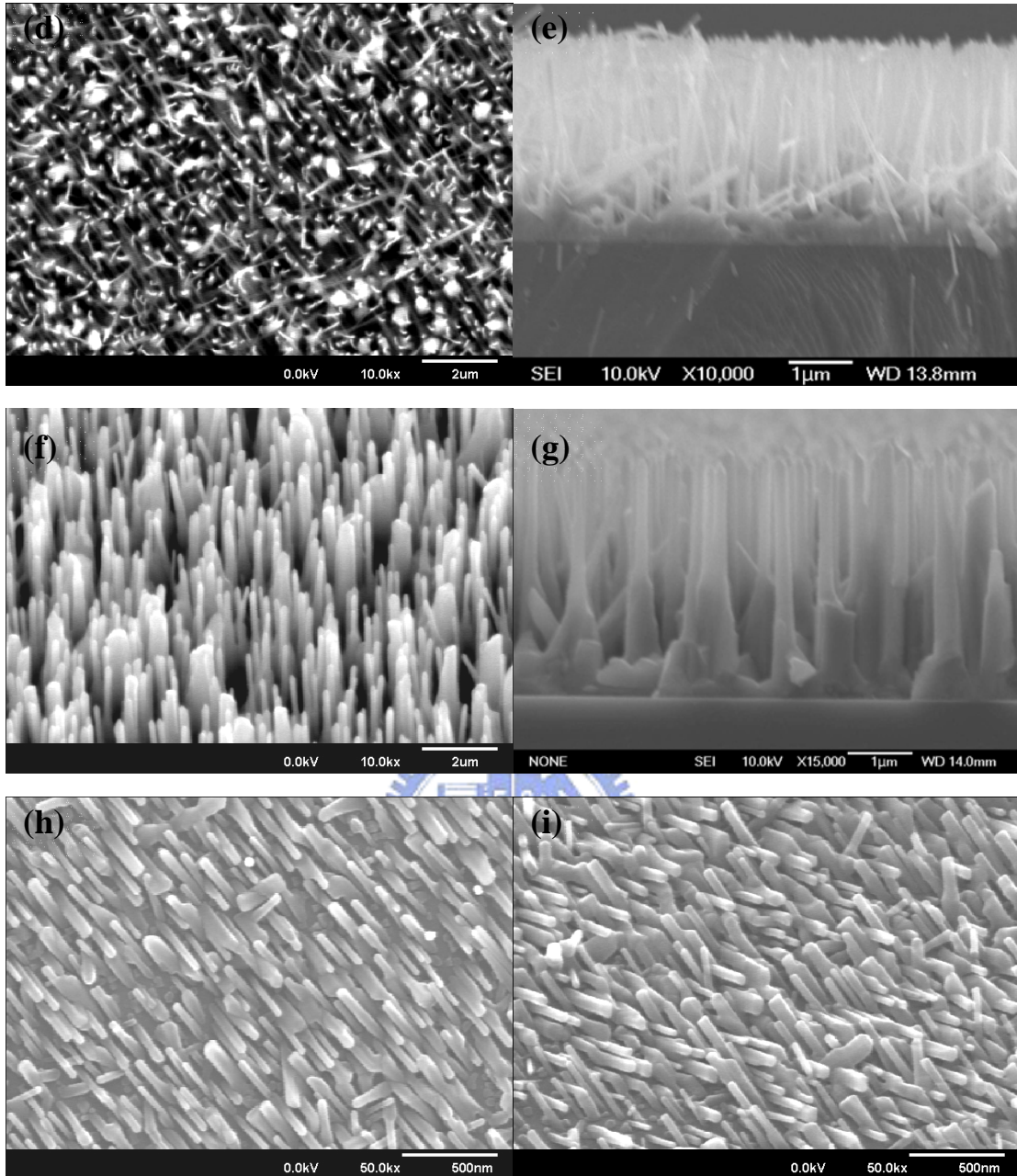
Fig. 4-3 (a) The top view of ZnO film, (b) (c) top view and cross-sectional images of ZnO nanowire ,

(d) (e) and (f) (g) top view and cross-sectional images of ZnO nanowire, (h) (i) top view and

side view of ZnO nanowire are fabricated from modified VS method at 460 ℃, 500 ℃, 520 ℃,

540 ℃ and 580 ℃

At low temperature at 460 ^{0}C, the ZnO prefers to grow 2-dimensionally as in Fig. 4-3 (a).   When the temperature was raised to 500 ℃, some nanorods were grown from the ZnO buffer layer as the top and side views in Fig. 4-3 (b) and (c).   In this case, the growth temperature may be still too low to grow well vertically aligned

nanowires, some of nanowires incline towards the surface of the substrate. At 520 ℃, one could observe more upright nanowires with diameter of ~70 nm grown on a buffer layer of ~300 nm thick [see top and cross section views in Fig. 4-3 (d) and (e)]. As the growth temperature being set at 540 ℃, we can obtain vertically aligned ZnO nanowires with diameter of ~100nm on a thinner buffer layer of ~ 100 nm. However, further raising the growth temperature to 580 ℃, we found the ZnO nanowires incline towards the surface of the substrate again as shown in Fig. 4-3 (h) and (i), respectively.
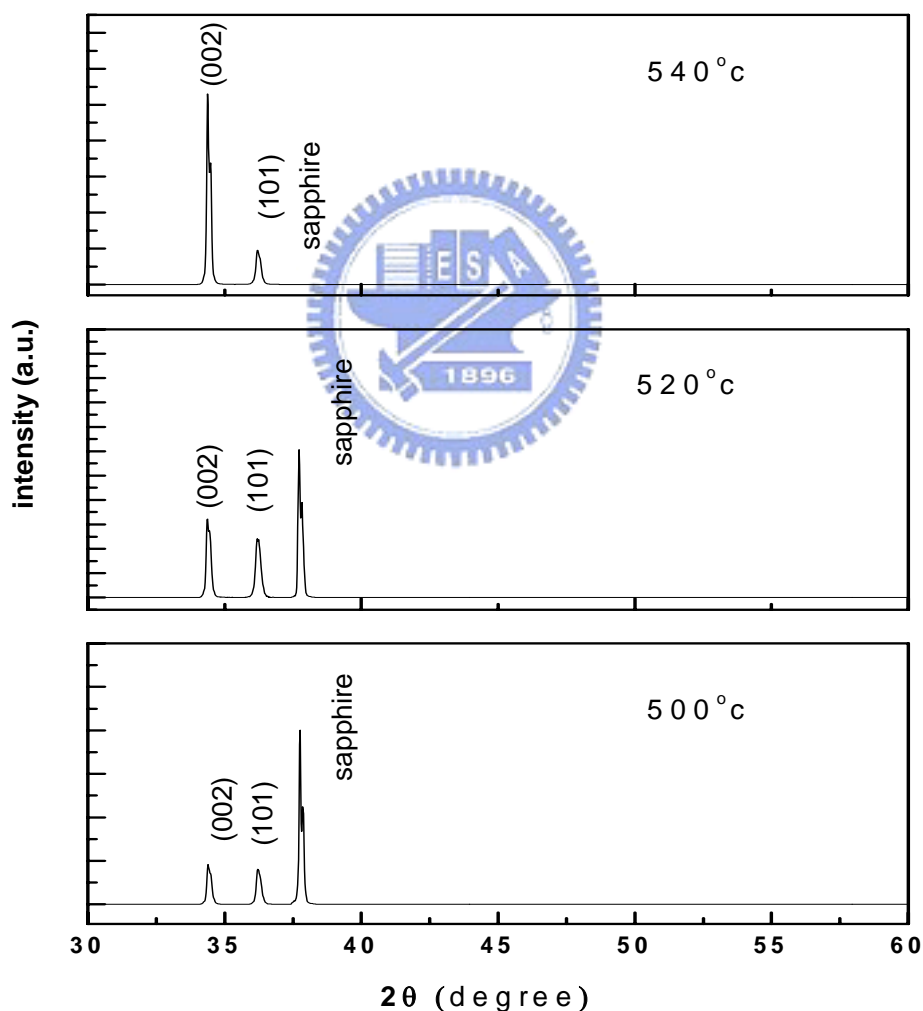

Fig. 4-4 The XRD pattern of ZnO depend on different growth temperature on a plane sapphire substrate.

The mechanism of which the ZnO nanowire is formed is attributed to the difference in growth rates in different crystalline directions. The growth rate being highest along the *c* axis [10]. From the XRD pattern of Fig. 4-4, we can see ZnO prefers to grow along (002) over (101) with increasing growth temperature. And the epitaxial relationship between ZnO nanowires and the substrate is the ZnO (001) plane grown on the sapphire (110) plane surface [12]. The ZnO preferred c-axis due to the relative growth rates of (002) > (101) > (100) [4, 11].
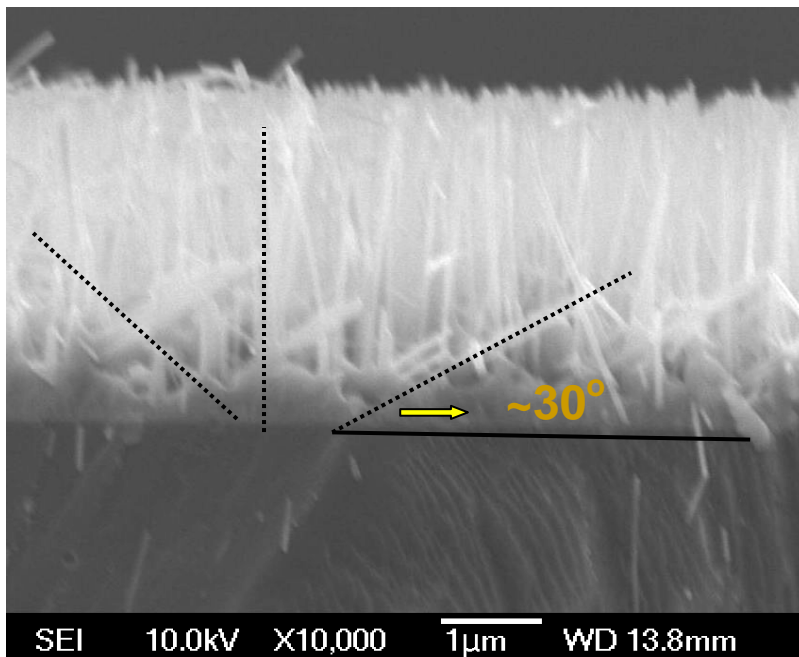

Fig. 4-5 The SEM cross-section image of ZnO nanowire at 520 ℃

Some of the wires were inclined ~30 degrees to the surface of substrate, e.g., for the 520 ℃ grown sample in Fig. 4-5. From the XRD in Fig. 4.4 we speculated that the inclineing wires should also grow along (002) but with their (101) plane aligning with the a-sapphire plane (110) [13, 14, 15]. In order to verify this concept, we calculated the angle between (002) and (101) planes using:

$$\cos \Phi = \frac{h_1 h_2 + k_1 k_2 + 0.5(h_1 k_2 + k_1 h_2) + (3a^2/4c^2)l_1 l_2}{[h_1^2 + k_1^2 + h_1 k_1 + (3a^2/4c^2)l_1^2]^{1/2}[h_2^2 + k_2^2 + h_2 k_2 + (3a^2/4c^2)l_2^2]^{1/2}} ,$$

(4-4)

where Φ is the angle between ($h_1 k_1 l_1$) and ($h_2 k_2 l_2$) planes and the formula is suitable for hexagonal structure, we get $\Phi = 61^o$. So the angle between the wires and substrate is 29°, which is close to the SEM observation. It had recently been reported that the substrate symmetry would influence the growth direction of wires, [13]. In our case, the a-plane sapphire has three symmetric planes as shown in Fig. 4-6 (a) and (b). The upright-growth wires should have their (002) plane aligned with sapphire (110) one, and the 30°–inclined wires should also align with the other 3-fold symmetric planes.
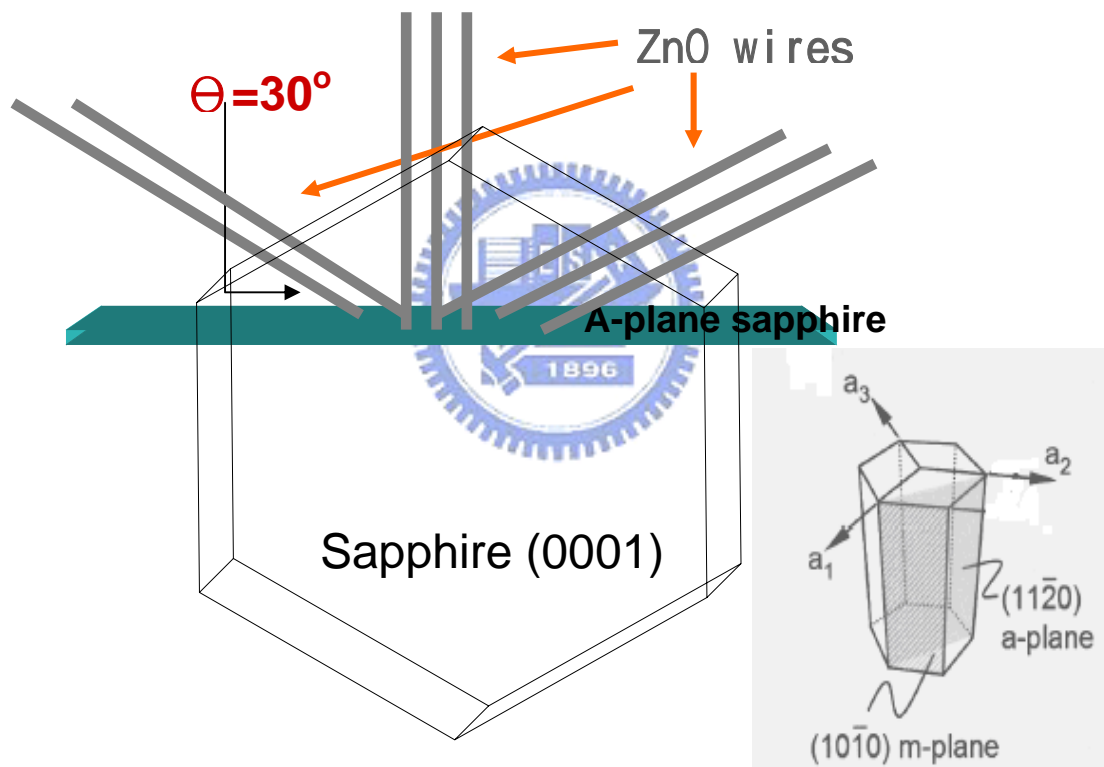

Fig. 4-6 A schematic shows the angular relationship between the m-plane and a-plane sapphire. [10]

4.2 Optical properties of ZnO nanowires

4.2.1 Room temperature PL spectra

The room temperature (RT) PL spectra of ZnO nanowires grown by the modified VS method were shown in Fig. 4-7. A strong UV emission peak having photon

energy of ~ 3.27 eV with FWHM of ~ 110 meV was observed accompanied with weak broad green band in the range of 1.9 eV~2.8 eV (wavelength = 440 nm ~ 650 nm). This sharp UV emission peak is attributed to the near band edge emission [16.17]. As comparison with ZnO bulk crystal (free exciton emission at 3.28 eV), the emission peak slightly shift toward the lower energy. Similar observation can be found in ZnO nanosaws that result from a mixture of free exciton and other impurity-related transitions [17] or due to the laser heating. The broad emission is the deep-level emission, which is attributed to the oxygen vacancy. The strong UV emission and weak green emission in PL spectra indicates that the ZnO nanosaws have a good crystal quality with few oxygen vacancies.
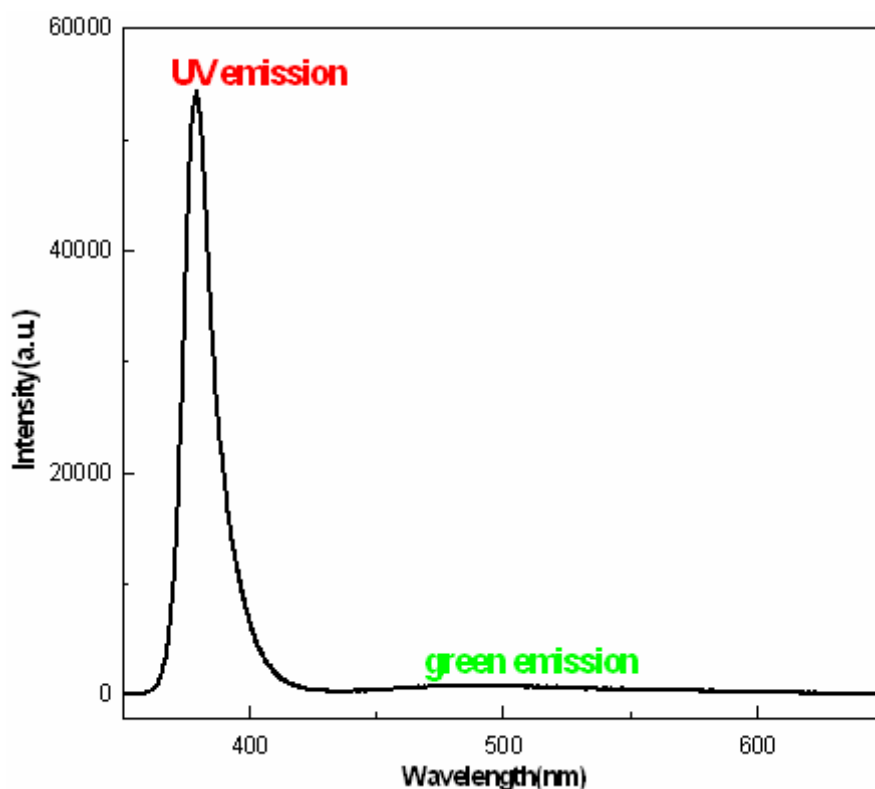

Fig. 4-7 The PL spectra of the ZnO nanowire measured at room temperature.

4.2.2 Low temperature PL spectrum

Figures 4-8 (a) and (b) show the low temperature PL spectra of ZnO nanowires

prepared by modified and conventional VS methods, respectively.   We can clearly see the free exciton and bound exciton peaks.   By using the "peak-fit" software to decompose every peak in near band edge emission, we could determine the ZnO nanowire quality based on the intensity ratio (I_{FX}/I_{BX}) of the free exciton to the bound exciton emissions. I_{FX}/I_{BX} = 10.3% and 3.76% that show the ZnO nanowires grown by the modified VS method have better crystal quality.

The sample prepared by the conventional VS method would have thick buffer layer which formed at the lower growth temperature.   It was reported that low substrate temperature or high growth pressure would tend to form the thin-film structure [18] ,and the thin-film structure formed at a lower temperature was amorphous or polycrystalline [19].   For the objective of manufacturing nano-device such as buffer-layer with low quality and uncontrollable thickness is undesirable.   It would be desirable to use specific thin film with good quality as the buffer layer between the nanowire structure and the substrate.   For example the ZnO thin film with Al doping can be the used as n-type transparent electrode.
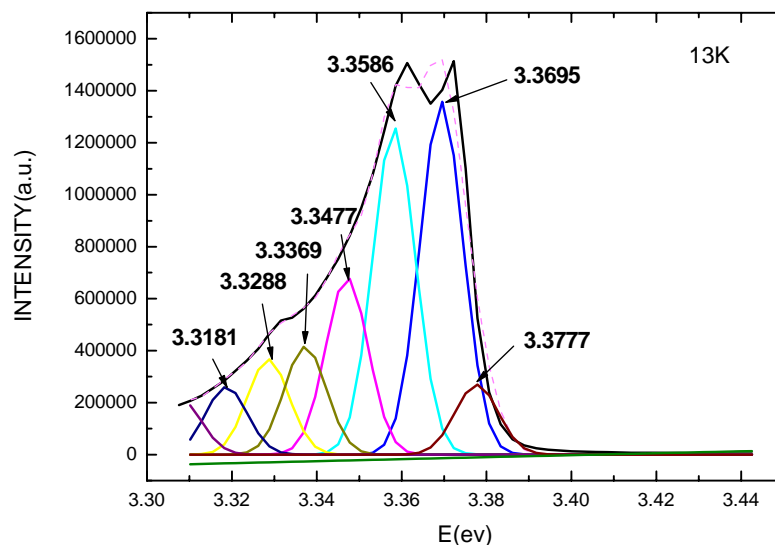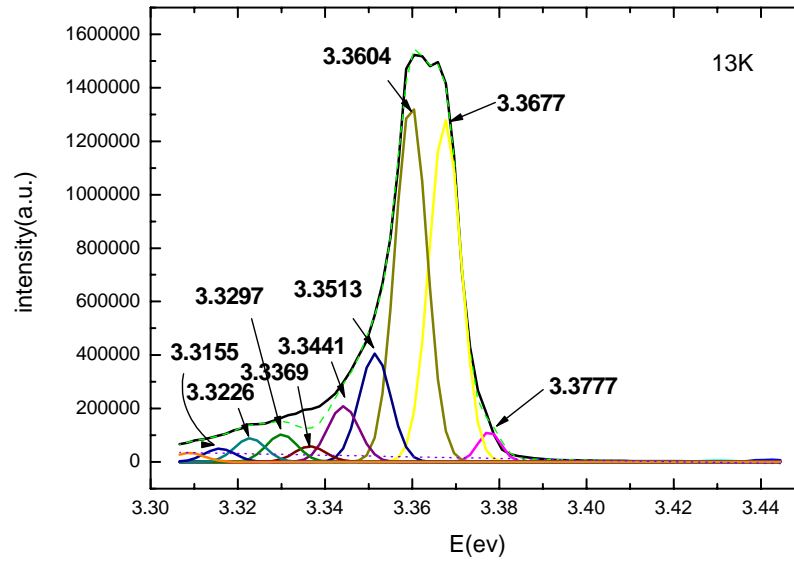
Fig. 4-8　The low temperature PL spectra of samples grown with the same conditions by using modified VS method (a) and conventional VS method (b), respectively.

In ZnO sample grown by modified VS method at 540 ℃, we observe the PL spectra at 13 K. The low-temperature PL spectra show Fig. 4-9 are dominated by several close lying bound excitons in the range from 3.358 to 3.366 eV. According to the literature [21], the peak is attributed to the neutral shallow donor-bound exciton because of the presence of donor due to unintentional impurities and shallow donor-like defects. The recombination of bound excitons typically gives rise to sharp lines with a photon energy characteristic to each defect. The free exciton peak is at 3.377 eV and the region of 3.320 to 3.330 eV is attributed to the neutral donor-bound exciton transition and the two-electron satellite (TES) transition. TES transition involves radiative recombination of an exciton bound to a neutral donor leaving the donor in the excited state. The energy difference between the ground-state neutral donor-bound excitons and its TES state can be used to determine the donor binding energy [22, 23]. The donor excitation energy from the ground

39

state to the first excited state equals to 3/4 of the donor binding energy near 50 meV. The LO-phonon replicas occur with a separation of 71~73 meV, which corresponds to the LO-phonon energy in ZnO. [24]   There are small energy spacing of FX-1LO replica due to create an exciton-polaron at ~64 meV, and no shift for BX-LO replicas as well as FX-2LO, and FX-3LO that corresponds to 71~73 meV. [25] We observe a radiative recombination peak at 3.220 eV that is attributed to the donor-acceptor pair. [21, 26]

.With the increasing sample temperature, its intensity drops, and an adjacent line at 3.234 eV on the high energy side gains intensity as show Fig. 4-10.   This temperature dependence is typical for DAP transitions turning into free electron-acceptor transition when the donors are thermally ionized with the temperature increasing.   But the FX-2LO peak at 3.233 eV is close to electron-acceptor peak, with the temperature increasing to near 100 K the phonon replicas is drop [27] and the electron-acceptor peak is appeared at the temperature higher than 40 K.   The temperature above 70 K the phonon replicas effect is down and the electron-acceptor is more important, so at 70 K the peak near 3.23 eV is dominated by electron-acceptor.

We analyzed the integral intensity in the UV region. The integral PL intensity usually decreases with temperature due to the thermal quenching as [28, 29]

$$I_{(T)} = \frac{I_0}{1 + A\exp(-\frac{E_a}{k_B T})} \quad , \tag{4-5}$$

Where I_0 is the peak intensity at 0 K, A is a parameter, E_a is the activation energy in the thermal quenching process, and k_B is Boltzmann constant, and we fit the measured $I_{(T)}$ by (4-5) and get the activation energy of 54.6 meV which is closed to the ZnO free exciton binding energy 60 meV as shown in Fig. 4-11.
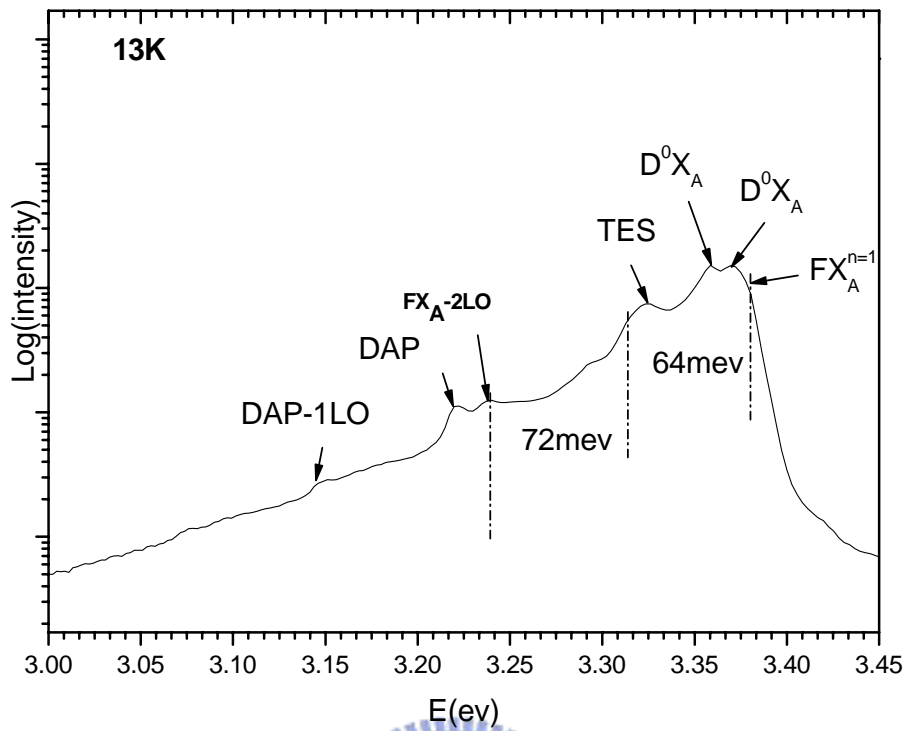
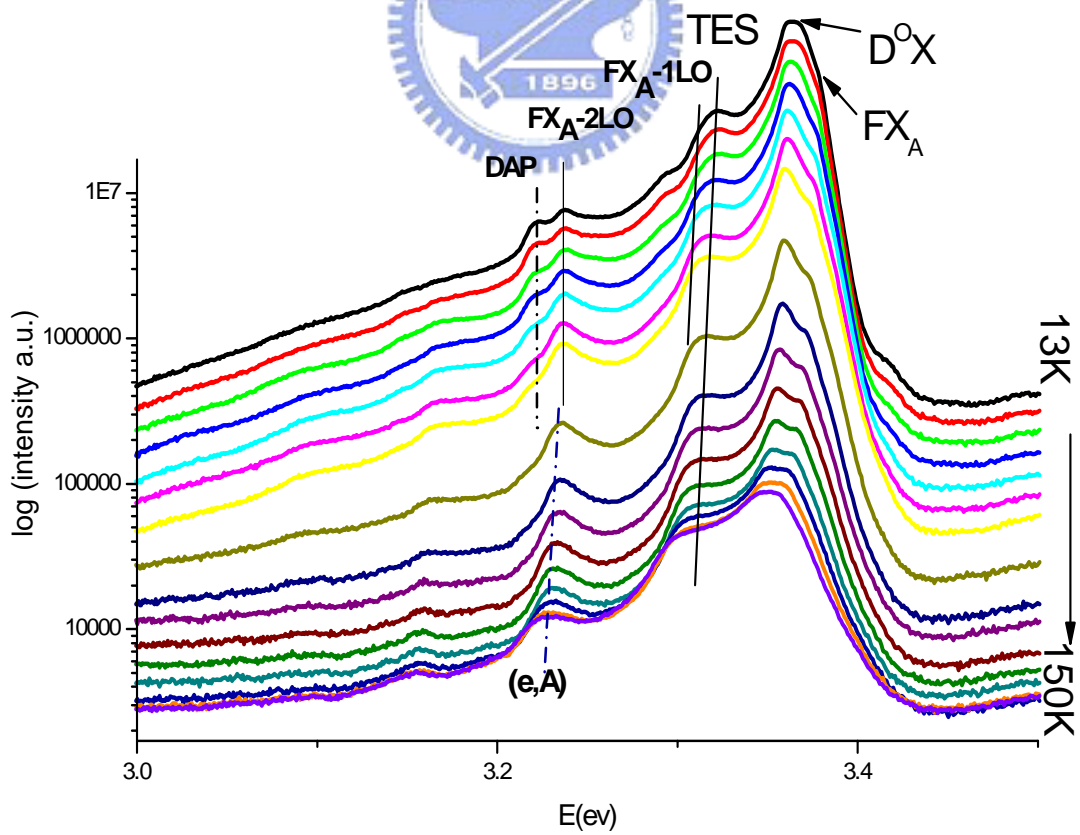Fig. 4-9 PL overview spectrum of ZnO sample recorded at 13K.

Fig. 4-10 Series of low temperature PL spectra of the ZnO sample recorded at different temperature.

Between 13 and 150 K the donor-acceptor pair transition at 3,22 eV decrease, and the adjacent band-acceptor transition at 3.234 eV increase.
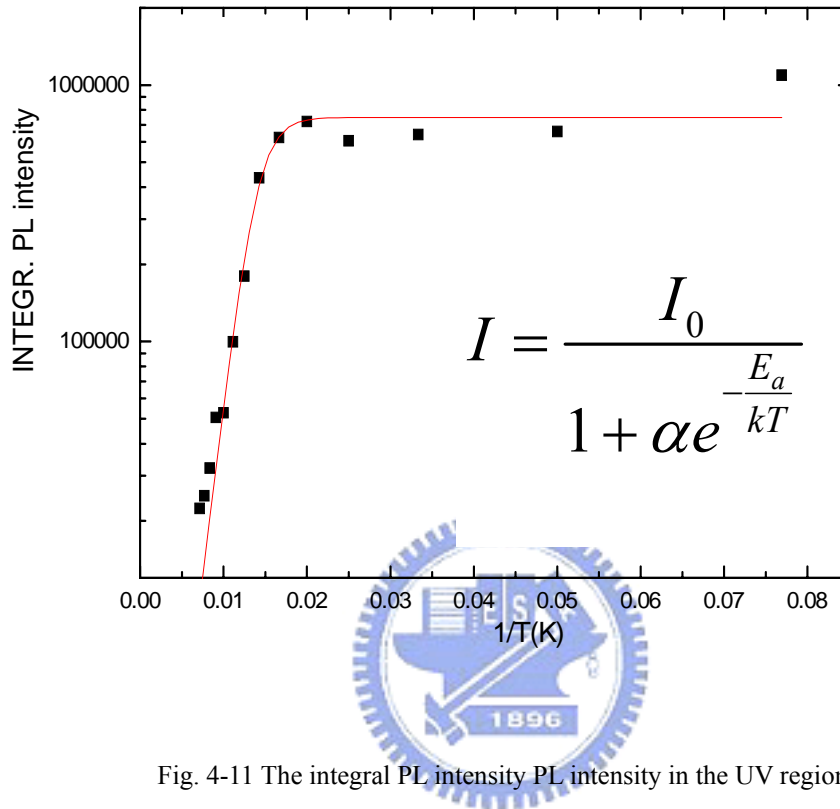

$$I = \frac{I_0}{1 + \alpha e^{-\frac{E_a}{kT}}}$$

Fig. 4-11 The integral PL intensity PL intensity in the UV region.

4.2.3 Raman spectra

The wurtzite structure of ZnO belongs to the space group C_{6mm} (C_{6v}^4) with two formula units in a primitive cell. [31, 32]   The group theory predicts the existence of the following optic modes: $A_1+2B_1+E_1+2E_2$ at the Γ point of the Brillouin zone; B_1(low) and B_1(high) modes are normally silent; A_1, E_1, and E_2 modes are Raman active; and A_1 and E_1 are also infrared active.   To analyze the Raman mode of ZnO materials on sapphire substrate has to be quite careful because there are several peaks overlapped with each other. [33]   In spite of two features in Raman spectra, we still observe the E_2(high) mode at 436 cm^{-1} with their width of 10 cm^{-1} indicating good

crystal quality, we also observed very weak $E_1(LO)$ mode near 584 cm^{-1} for the Fig. 4-8. This is because the propagation direction of the $E_1(LO)$ parallel to [0-11] is parallel neither to the XY-plane nor to the Z-axis. [34]

A typical micro-Raman spectrum for ZnO nanowires grown on a-plane sapphire substrate by modified VS method at 540 ℃ are shown in Fig. 4-8(b). The observed phonon frequency is $E_2(high)$ at 436 cm^{-1}. Since the penetration depth of the Argon laser is longer than the ZnO nanowires, pronounced phonon modes of the sapphire substrate at 380 cm^{-1} and 416 cm^{-1} were not observed, because the micro-Raman system focused the light on the surface of sample that only get the surface information. The $E_1(LO)$ is associated with a lattice defect, such as oxygen vacancies and zinc interstitial in the ZnO nanowires, which is similar to the previous results. [30] Clearly, this result with weak $A_1(LO)$ indicates that the sample is composed of the ZnO with high quality hexagonal nanowires. With the temperature increasing, the $E_2(high)$ peak was elevated and the substrate information diminished. At 580^{0}C the ZnO nanowires was to thin so we can observed the sapphire substrate message, we can inspected the $A_1(LO)$ peak at ~574 cm^{-1} that the inclined nanowires shown as Fig. 4-12 (a).
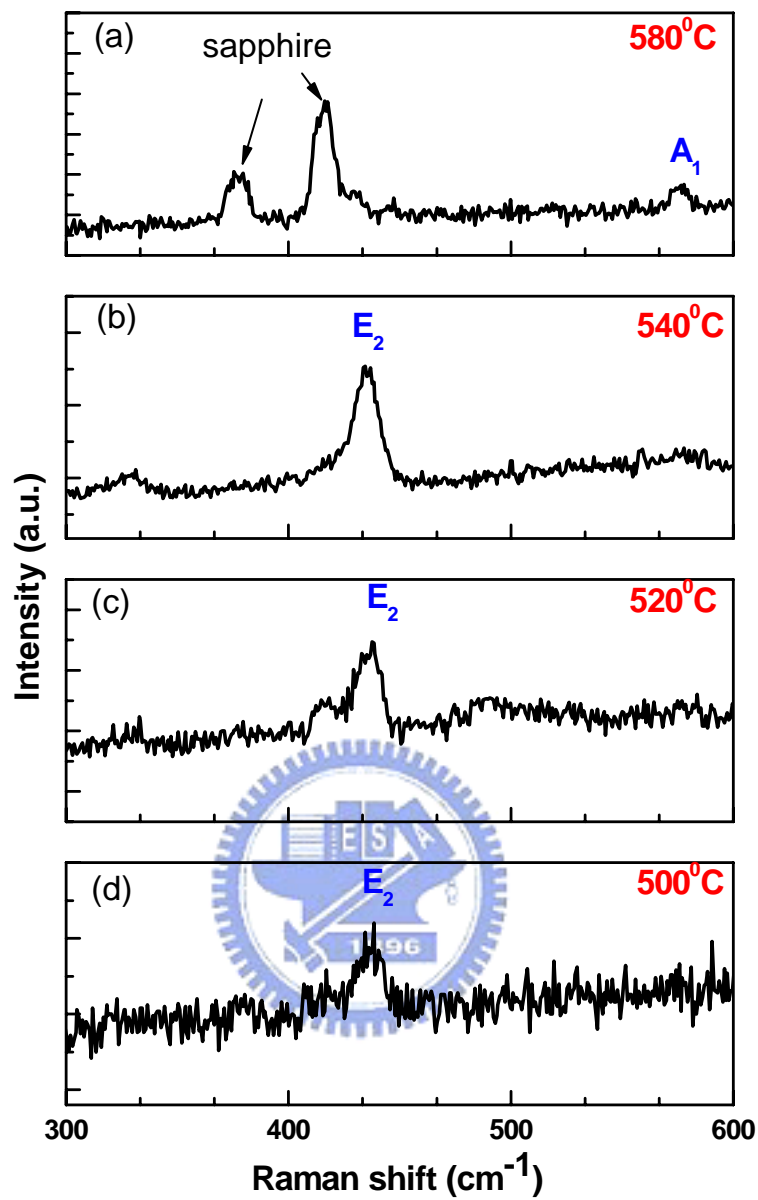
Figure. 4-12 micro-Raman spectra of the ZnO nanowires were grown on sapphire substrate at different

temperature.

References

[1] H.C. Hsu, Y.K. Tseng, H.M. Chang, J.H. Kuo, W.F. Hsieh, *J. Crystal Growth*, **261**, 520 (2004).

[2] A Colli, A Fasoli, S Hofmann, C Ducati, J Roberston and A C Ferrari, *Nanotechnology* **17,** 1046-1051 (2006)

[3] J. Lu, *Appl. Surface Sci.*, **207**, 295, (2003)

[4] D. C. Kim, B. H. Kong, H. K. Cho, D. J. Park and J. Y. Lee, *Nanotechnology,* **18,** 015603 (2007)

[5] N. Pan, X. Wang, K. Zhang, H. Hu, B. Xu, F. Li and J. G. Hou, *Nanotechnology,* **16,** 1069-1072 (2005)

[6] Y. H. Leung, A. B. Djurisic, J. Gao, M. H. Xie, S. J. Xu, W. K. Chan, *Chem. Phys. Lett.*, **394**, 452 (2004)

[7] Z. L. Wang, X. Y. Kong, J. M. Zuo, *Phys. Rev. Lett.*, **91**, 185502-1 (2003)

[8] A Colli, A Fasoli, SHofmann, C Ducati, J Robertson and A C Ferrari, *Nanotechnology,* **17**, 1046–1051 (2006)

[9] S. H. Dalal, D. L. Baptista, K BKTeo, R. G. Lacerda, D. A. Jefferson, and W. I. Milne, *Nanotechnology,* **17**, 4811–4818 (2006)

[10] S. Muthukumar, H. Sheng, J. Zhong, Z. Zhang, N. W. Emanetoglu, and Y. Lu, *IEEE Trans. Nanotechnology*, **2**, 50   (2003).

[11] Baxter J B and Aydil E S 2005 *J. Cryst. Growth,* **274,** 407

[12] B. P. Zhang, N. T. Binh, and Y. Segawa, Y. Kashiwaba and K. Haga,   *Appl. Phys. Lett.*,**84**, 26

[13] H.T. Ng, B. Chen, J. Li, J. Han, M. Meyyappan, J. Wu, S.X. Li, E.E. Haller, *Appl. Phys. Lett., 82, 13 (2003)*

[14] M. H. Huang, S. Mao, H. Feick, H. Yan, Y. Wu, H. Kind, E. Weber, R. Russo, and P. Yang, *Science* **292**, 1897 (2001).

[15] Peidong Yang *et al. Adv. Funct. Mater. 2002, 12,* No. 5

[16] H.C. Hsu, Y.K. Tseng, H.M. Chang, J.H. Kuo, W.F. Hsieh, *J. Crystal Growth*, **261**, 520 (2004).

[17] B.P. Zhang, N.T. Binh, Y. Segawa, Y. Kashiwaba, K. Haga, *Appl. Phys. Lett,*. **84** 586 (2004).

[18] Sun-Hong Park, Seon-HyoKim1 and Sang-Wook Han, *Nanotechnology* **18** (2007) 055608.

[19] Min-Chang Jeong, Byeong-Yun Oh, Moon-Ho Ham, and Jae-Min Myounga, *Appl. Phys. Lett,* 88, 202105.

[20] N Pan et al. *Nanotechnology* 16 1069-1072 (2005).

[21] A. Teke et al. *Phys. Rev. B* 70, 195207 (2004).

[22] K. Thonke, Th. Gruber, N. Teofilov, R, Schonfelder, A. Waag, and R. Sauer, *Physica B* 308-310, 945 (2001).

[23] H. Alves, D. P. Sterer, A. Zeuner, T. Riemann, J. Christen, D. M. Hofmann, and B. K. Meyer, *Opt. Mater*. 23, 33 (2003).

[24] Y. P. Varshni, Physica (Amsterdam) 34, 149 (1967); L. Wang and N. C. Giles, *J. Appl. Phys*. 94, 973 (2003).

[25] H.-C. Hsu *et al., Solid State Commun.* 131, 371 (2004).

[26] K. Thonke et al. *Physica B* 308-310 (2001) 945-948.

[27] C. F. Klingshirn, *Semiconductor Optics* (Springer, Berlin).

[28] D. S. Jiang, H. Jung, and K. Ploog, *J. Appl. Phys*. 64, 1371 (1988).

[29] Fonoberov et al. *Phys. Rev. B* 73, 165317 (2006).

[30] J. J. Wu and S. C. Liu, *J. Phys. Chem. B*, **106**, 9546 (2002)

[31] J. M. Calleja and M. Cardona, *Phys. Rev. B,* **16,** 3753 (1977)

[32] F. Decremps, J. Pellicer-Porres, A. M. Saitta, J. C. Chervin, A. Polian, *Phys. Rev.*

B **65**, 092101 (2003)

[33] N. Ashkenov, B. N. Mbenkum, C. Bundesmann, V. Riede, M. Lorenz, D.

Spemann, E. M. Kaidashev, A. Kasic, M. Schubert, M. Grundmann, G. Wagner,

H. Neumann, V. Darakchieva, H. Arwin, and B. Monemar, *J. App. Phys.*, **93,** 126

(2003)

[34] C. A. Arguello, D. L. Rousseau, and S. P. S. Porto, *Phys. Rev.,* **181**, 1351 (1969)

Chapter 5 Conclusion and future works

5.1 Conclusion

In summary, ZnO nanostructures had been successfully grown by a vapor transport process. Preheating the substrate before supplying the Zn source provide an alternative way of growing better quality ZnO nanostructures than the conventional VS method. The results of XRD and PL measurements indicate that the ZnO nanostructures possess single-crystal structure with wurtzite phase. The growth mechanism of the nanowires is suggested to be the self-catalyst process for the growth of oxide nanostructures without the existence of external metallic catalysts. With controlled growth temperature can deterministic synthesis of ZnO nanostructure morphology and diminish the thick of buffer layer that will benefit to make ZnO device with one dimension nanostructure by using modified VS method. The ZnO nanowires exhibit strong UV emission and weak green emission, indicating very good crystal quality. At low temperature the higher free exciton emission than that of bound exciton reveals that the modified VS method can grow better quality nanowires than the conventional VS method.

5.2 Future works

In the current research on ZnO-based nanostructures, our major goal is to grow ZnO-based nanostructures and analyzing their optical properties. In the future, we would try to make hetero-nanostructures, such as multiple quantum wells in a nanowire or multiple core/shell structured nanowires by using modified VS method. It is an important issue for the development of the ZnO-based nanoscale devices. Besides, we propose using the near field scanning optical microscope (NSOM) or

cathodoluminescence (CL) to study the spatial resolved photon emission and laser action from nanowires. Finally, for the applications of nanoscale devices, developing technology for large-scale fabrication of oriented and well-aligned ZnO-based nanostructures is necessary.